[Lys(−2)-Arg(−1)]Endothelin-1 Solution Structure by Two-Dimensional ^{1}H-NMR: Possible Involvement of Electrostatic Interactions in Native Disulfide Bridge Formation and in Biological Activity Decrease

André Aumelas,*,‡ Laurent Chiche,‡ Shigeru Kubo,§ Naoyoshi Chino,§ Haruhiko Tamaoki,|| and Yuji Kobayashi||

Centre de Biochimie Structurale CNRS UMR C9955, INSERM U414, Faculté de Pharmacie, 34060 Montpellier Cedex 1, France, Peptide Institute, Inc., 4-1-2 Ina, Minoh-Shi, Osaka 562, Japan, and Institute for Protein Research, Osaka University, 3-2 Yamadaoka, Suita Osaka 565, Japan

Received November 7, 1994; Revised Manuscript Received January 3, 1995[⊗]

ABSTRACT: Addition of the Lys(−2)-Arg(−1) dipeptide, present in the precursor protein, to the N-terminus of endothelin-1 (ET-1), to form a 23-residue peptide (KR-ET-1) has been shown to greatly improve formation of native disulfide bridges and to dramatically decrease biological activity. Conformational analysis was carried out on this peptide. During protonation of the carboxyl groups, CD spectra showed a decrease in the helical contribution, and NMR spectra displayed strong chemical shift modifications, suggesting the importance of electrostatic interactions in the KR-ET-1 conformation. CD spectra and two-dimensional NMR experiments were performed to investigate the KR-ET-1 three-dimensional structure in water in the carboxylic acid and carboxylate states. Distance and angle constraints were used as input for distance geometry calculations. The KR-ET-1 carboxylic acid conformation was found to be very similar to ET-1, with a helix spanning residues 9−15 and an unconstrained C-terminal part. In contrast, in the carboxylate state, large changes in Arg(−1) and Phe14 chemical shifts and long-range NOEs were consistent with a conformation characterized by a helix extension to Leu17 and a stabilized C-terminal section folded back toward the N-terminus. In addition, thanks to NOEs with Cys11 and Phe14, the Arg(−1) side chain appeared well-defined. Simulated annealing and molecular dynamics calculations, supported an Arg(−1)−Glu10 salt bridge and an electrostatic network involving the charged groups of Trp21, Asp18, and Lys(−2). Moreover, stabilization of the KR-ET-1 C-terminal part is probably reinforced by hydrophobic interactions involving the Val12, Tyr13, Phe14, Leu17, Ile19, Ile20, and Trp21 side chains. *In vitro*, native disulfide bond formation improvement observed for KR-ET-1 could be ascribed to electrostatic interactions and more specifically to the Arg(−1)−Glu10 salt bridge. *In vivo*, similar interactions could play an important role in the native folding of the ET-1 precursor protein. On the other hand, modification in the environment and a reduced mobility of the KR-ET-1 Trp21 key residue, when compared to ET-1, could explain, at least in part, the strong decrease in biological activity.

ET-1[1] is a potent long-lasting vasoconstrictor peptide of 21 residues isolated from aortic endothelial cells. It results from the degradation of pre-proendothelin (203 residues) by various endopeptidases to give proendothelin first and then big endothelin (38-residue peptide). Next, the Trp21−Val22 amide bond in big ET-1 is cleaved by an endothelin converting enzyme to produce the bioactive ET-1 molecule whose structure is stabilized by two disulfide bonds (Cys1−Cys15 and Cys3−Cys11) (Yanagisawa et al., 1988a,b; Erhardt, 1992; Phillips et al., 1992).

In ^{1}H-NMR experiments, aggregation of ET-1 has been observed in aqueous solutions with concentrations in the range of 1−4 mM; this aggregation is probably due to a cluster of several hydrophobic residues mainly located in the C-terminal part (Bennes et al., 1990). To overcome this problem, various organic solvents (acetic acid, ethylene glycol, methanol) were added to water. The results of the different conformational studies carried out with these solvent mixtures were consistent with a helical conformation spanning residues 9 through 15 (Tamaoki et al., 1991; Andersen et al., 1992; Reily & Dunbar, 1991; Aumelas et al., 1991a; Labhardt & Grunauer, 1990; Krystek et al., 1991). The 1−4 extended part is linked to the helical motif by two disulfide bridges (Cys1−Cys15 and Cys3−Cys11), giving the cystine-stabilized helical motif (Tamaoki et al., 1992, 1991; Kobayashi et al., 1991; Mihara et al., 1994). It has been shown, however, that the helical part is still conserved in the monocyclic 3−11 disulfide bond analogue (Coles et al., 1994). Recently, ET-1 crystals containing six molecules per

* Author to whom correspondence should be addressed.
‡ Centre de Biochimie Structurale CNRS UMR C9955.
§ Peptide Institute, Inc.
|| Institute for Protein Research.

⊗ Abstract published in *Advance ACS Abstracts,* March 15, 1995.

[1] Abbreviations: CD, circular dichroism; 1D and 2D, one and two dimensional; TSP-d_4, sodium 2,2,3,3-tetradeuterio-3-(trimethylsilyl)-propionate; acetic acid-d_4, tetradeuterated acetic acid; DG, distance geometry; DQF-COSY, 2D double-quantum-filtered correlation spectroscopy; ET, ET-1, ET-2, and ET-3, endothelin; FID, free induction decay; GSH and GSSG, reduced and oxidized glutathione; MD, molecular dynamics; Nle, norleucine; NMR, nuclear magnetic resonance; NOE, nuclear Overhauser effect; NOESY, 2D nuclear Overhauser effect spectroscopy; RMSD, root mean square deviation; ROESY, rotating-frame Overhauser effect spectroscopy; RP-HPLC, reverse-phase high-performance liquid chromatography; SA, simulated annealing; STX, sarafotoxin; TOCSY, total correlation spectroscopy; VIC, vasoactive intestinal contractor peptide; $d_{NN}(i,j)$, NOE connectivities between the NH proton of residue i and the NH proton of residue j; $d_{\alpha N}(i,j)$, NOE connectivities between the Cα proton of residue i and the NH proton of residue j; $d_{\alpha\beta}(i,j)$, NOE connectivities between the Cα proton of residue i and the Cβ proton of residue j.

0006-2960/95/0434-4546$09.00/0

FIGURE 1: KR-ET-1 sequence. For the sake of clarity, the ET-1 numbering has been conserved, and negative numbers were given to the N-terminal dipeptide as follows: Lys(−2), Arg(−1). The disulfide bridges are indicated by lines connecting cysteines.

asymmetric unit were obtained in aqueous solution (Peapus et al., 1993). The X-ray structure solved at 2.18 Å by Janes et al. (1994) showed, in addition to the cystine-stabilized helical motif, a helical conformation of the 16−21 C-terminal tail that has never been observed in NMR solution structures.

We thought that the aggregation problem could be overcome by addition of new charged residues. We therefore synthesized a modified ET-1 peptide in which the N-terminus was extended by the Lys(−2)-Arg(−1) basic dipeptide present in the pre-pro-ET-1 sequence (Yanagisawa et al., 1988a), resulting in the 23-residue peptide designated KR-ET-1 (Figure 1). A different basic dipeptide, Arg(−2)-Arg(−1) is found in ET-2, ET-3, and VIC precursors (Saida et al., 1989; Inoue et al., 1989).

The ET-1 folding reaction yields *in vitro* a 3/1 ratio of native disulfide bonds (Cys1−Cys15 and Cys3−Cys11) to non-native ones (Cys1−Cys11 and Cys3−Cys15) (Yanagisawa et al., 1988b; Kumagaye et al., 1988). The big ET-1 folding reaction has been shown to yield a similar native/non-native disulfide arrangement ratio (Gaeta et al., 1990; Kubo et al., manuscript in preparation). In contrast, for KR-ET-1 the ratio was significantly improved; it is 9/1 and even reaches 24/1 in the presence of redox reagents. This improvement is abolished when the oxidation reaction is performed in the presence of guanidine hydrochloride. These folding differences will be fully described elsewhere (Kubo et al., manuscript in preparation). The biological activity of KR-ET-1 has been reported to be 540-fold lower than that of ET-1 itself (Nakajima et al., 1989a,b). To investigate the structural changes induced by addition of the dipeptide Lys(−2)-Arg(−1) at the N-terminus, conformational analyses were carried out on KR-ET-1.

In this paper, we report the solution structure of KR-ET-1 determined in the carboxylic acid and in the carboxylate states. The carboxylic acid conformation appeared very similar to ET-1, whose structure is pH independent. In contrast, the KR-ET-1 carboxylate conformation displayed significant structural modifications probably induced by electrostatic interactions. The possible implications of these interactions in the disulfide bond formation improvement and in the decrease of biological activity are discussed.

MATERIALS AND METHODS

Synthesis. The synthesis of ET-1 and KR-ET-1 peptides was carried out according to the previously described scheme (Nakajima et al., 1989b; Kumagaye et al., 1988). ET-1 and KR-ET-1 reduced peptides were obtained by treating the corresponding oxidized peptides with a 10−30-fold molar excess of dithiothreitol in 0.1 M ammonium acetate buffer at pH 9.5 for 10 min. All the reduced peptides were stored in a freezer under a nitrogen atmosphere after purification by gradient elution RP-HPLC using CH_3CN in 0.1% TFA.

Circular Dichroism. CD spectra of ET-1 and KR-ET-1 were recorded at 25 °C on a JASCO J720 spectrophotometer using a 1-mm path-length cell. Peptide solutions at a concentration of 0.02 mM were prepared, and three spectra were recorded at pH 9.5, 4.0, and 1.5. Each spectrum was scanned from 195 to 250 nm and accumulated for 32 scans.

NMR Spectroscopy. (A) Sample Preparation. ^2H_2O (99.95%) and acetic acid-d_4 were purchased from the CEA (Saclay, France). All pHs were measured in the NMR tube at room temperature with a 3-mm electrode and are given uncorrected for the deuterium effect. Lyophilized KR-ET-1 (4 mg) was dissolved in 0.45 mL of water containing 5% ^2H_2O for the lock signal. The peptide concentration of the resulting sample was about 3.2 mM. The pH was adjusted to 4.1 by addition of 0.1 N HCl. TSP-d_4 was added as an internal chemical shift reference at 0 ppm. A second sample of 4 mg was prepared in 99.95% deuterated water for both amide proton kinetic exchange and titration experiments (initial pH = 4.8). A third sample of 4.8 mg of KR-ET-1 was prepared with 0.45 mL of the 10/90 acetic acid-d_4/water mixture (v/v). The pH of this last sample was 2.5.

(B) NMR Experiments. NMR experiments were performed on two Bruker AMX spectrometers, operating at 500 and 600 MHz for the ^1H nucleus and processed with the UXNMR software.

2D DQF-COSY (Rance et al., 1983), TOCSY (Bax & Davis, 1985a), and NOESY (Macura et al., 1981) spectra were acquired in the phase-sensitive mode using time-proportional phase incrementation. Typically, 512 FIDs of 2048 time domain data points were collected except for DQF-COSY experiments for which better resolution was needed (800 FIDs of 4096 time domain data points). A spectral width of 8500 Hz was used in both dimensions. The residual water peak was suppressed by applying a continuous low-power irradiation pulse from the transmitter during the relaxation delay of 1 s and during the NOESY mixing time. TOCSY were recorded with a spin lock of 64 ms and NOESY with a mixing time of 100 and 180 ms. One zero filling and a $\pi/4$ phase-shifted sine-bell window function were applied in both dimensions before Fourier transform. A baseline correction was performed with a five-order polynomial function. Chemical shifts were determined with reference to TSP-d_4 without pH correction.

For the study in water, 1D KR-ET-1 spectra were recorded at temperatures ranging from 280 to 310 K (pH 4.1, carboxylate form), and the 2D data sets were collected at 305 and 280 K. Then the pH was lowered to 1.5 (carboxylic acid form), and another 2D data set was recorded at 300 K. Two tables giving chemical shifts of KR-ET-1 in the carboxylate and carboxylic acid states are provided in the supplementary material section.

Amide proton−deuterium exchange was performed only for the carboxylate form at 290 K and pH 4.8. It was followed by (i) 1D spectra recorded at increasing times and (ii) a NOESY experiment to identify the remaining amide protons. Titration experiments were carried out with the same sample by recording spectra at various pHs ranging from 4.8 to 1.3 (uncorrected pH readings). The pH was adjusted by addition of small amounts of 10% DCl or NaOD solutions. During the titration of KR-ET-1, two DQF-COSY experiments were recorded at pH 2.9 and 1.3 to identify the aromatic protons of Phe14 and Tyr13 residues as well as protons of the Arg(−1) side chain. To check KR-ET-1 aggregation, the sample was diluted 10-fold (0.32 mM), and two spectra were recorded at pH 4.0 and 1.3.

For the study in the 10/90 acetic acid/water (v/v) mixture, 1D spectra were recorded at different temperatures ranging from 315 to 280 K, and the 2D spectra were recorded at

290 and 280 K. In addition, a ROESY (Bax & Davis, 1985b) experiment was recorded with a mixing time of 50 ms. After acidification to pH 1.3 by 1 N HCl, another 2D spectra set was recorded at 280 K.

$^3J_{NH-C\alpha H}$ coupling constants were measured from the fingerprint cross-peak contour plot of the DQF-COSY experiment with a digital resolution of 1.0 Hz. Reported values obtained from the contour plot are given without any correction and appear to be slightly overestimated due to line-width contribution. For example, in the carboxylate form, the Ser2 $^3J_{NH-C\alpha H}$ values of 11.2 and 9.1 Hz were obtained from the contour plot and from the 1D spectrum, respectively.

Distance Geometry Calculations. From NMR data recorded at pH 1.5 and 4.1 in water, distance geometry calculations were carried out using the DIANA program (Günther et al., 1991) running on a Hewlett-Packard HP735 workstation, with the standard minimization parameters. NOE cross-peak intensities were estimated by their contour levels in the 100- and 180-ms mixing time and classified into four categories. An empirical distance calibration was used to build a set of distance constraints. Upper distance bounds of 3.0, 4.0, 5.0, and 5.5 Å were assigned to strong, medium, weak, and very weak connectivities, respectively. A value of 2.3 Å was used for strong $d_{\alpha N}(i, i+1)$ connectivities. Lower distance bounds were taken as the sum of the van der Waals radii.

As no stereospecific assignment could be reached for methyl and methylene protons, pseudoatoms were used after appropriate corrections of the constraints (Wüthrich et al., 1983; Wüthrich, 1986). Disulfide bridges were introduced through constraints of 2.0−2.1 Å on the S*i*−S*j* bonds and 3.0−3.1 Å on the S*i*−Cβ*j* and S*j*−Cβ*i* distances across the bridges. The $\chi 3$ dihedral angles were set to ±80−100° through Cβ*i*−Cβ*j* distance constraints of 3.75−3.95 Å.

In the carboxylate distance geometry calculations, depending on whether the $^3J_{NH-C\alpha H}$ coupling constants were high (≥9.0 Hz) or low (≤6.8 Hz), five ϕ angles [Arg(−1), Ser5, Asp8, Leu17, and Ile20] were forced between −90° and −150° and four ϕ angles (Ser4, Lys9, Val12, and Tyr13) between −30° and −90°. Although five amide protons were probably involved in hydrogen bonding, because of their slow exchange, no explicit hydrogen bond constraints were included in the calculations since the carbonyls involved were not unambiguously identified. From 271 initial distance constraints, 179 significant proton−proton distances were effectively used by the DIANA program and were distributed as follows: 42 intraresidual, 57 sequential, 46 medium range (*i*, *i*+2 and *i*+3), and 34 long range (*i*, ≥i+4). A total of 1000 calculations were performed, and on the basis of the target function values, the 10 best structures were retained.

Distance geometry calculations related to the carboxylic acid form were carried out, without ϕ angle constraints, by using 109 significant proton−proton distances (from 175 initial distance constraints), distributed as follows: 28 intraresidual, 49 sequential, 20 medium range (*i*, *i*+2 and *i*+3), and 12 long range (*i*, ≥*i*+4). A total of 1000 calculations were performed, and on the basis of the target function values, the 10 best structures were retained.

The Insight II program (Biosym Technology Inc., San Diego) was used to display and compare the structures.

Molecular Mechanics and Molecular Dynamics Calculations. Energy minimizations and molecular dynamics simulations were carried out on the KR-ET-1 distance geometry structures obtained in the carboxylate state using the SANDER module of the AMBER 4.0 modeling package (Pearlman et al., 1991) running on a Hewlett-Packard HP735 workstation. The intrinsic strain energy was computed with the all-atom force field (Weiner et al., 1986), and the nonbonded cutoff was taken as 10 Å. To mimic solvent effects in simulations run *in vacuo*, a distance-dependent dielectric constant was used. During the molecular dynamics runs, the covalent bond lengths were kept constant by applying the SHAKE algorithm (van Gunsteren & Berendsen, 1977), allowing a 2-fs time step to be used. The nonbonded pair list was updated every 20 steps, and the temperature was regulated by coupling the system to a heat bath with a coupling constant of 0.2 ps. Pseudoenergy terms taking into account the NMR interproton distance restraints were defined as follows via four threshold distance values: *r*1, *r*2, *r*3, and *r*4. In all cases *r*1 and *r*2 were set to 1.5 and 1.8 Å, respectively. *r*3 was taken as the upper boundary used in DG calculations, and *r*4 was chosen as *r*3 + 0.5 Å. For an observed distance lying between *r*2 and *r*3, no restraint was applied. Between *r*1 and *r*2 or between *r*3 and *r*4, parabolic restraints were applied. Outside the *r*1−*r*4 range, the restraints were linear with slopes identical at parabolic slopes at points *r*1 and *r*4. This was done so that large distance violations could be corrected while avoiding too great restraint forces capable of inducing local structure distortions. Because no stereospecific assignment could be achieved for the methyl or methylene protons, an $\langle r^{-6}\rangle^{-1/6}$ averaging scheme was used instead of pseudoatoms. The force constant for the NMR restraints was 32 kcal·mol^{-1}·Å^{-2}, except at the start of the simulated annealing process during which the value was raised from 3.2 to 32 kcal·mol^{-1}·Å^{-2} in 7 ps so that the structure could adapt more easily to the constraint potential.

Simulated Annealing Refinement. The 10 best DIANA structures were first energy minimized for 5000 cycles. These structures were then submitted to a 30 ps long simulated annealing. The temperature was raised from 10 to 900 K in 6 ps, maintained at this value for 10 ps, then slowly lowered to 300 K in 8 ps, and maintained at this latter value for 6 ps. A final energy minimization was performed (Hurle et al., 1992). The resulting structures are referred to later as the SA structures. After fitting all SA structures to the first one (backbone atoms of residues 1−3 and 9−16), an average SA model was computed by coordinate averaging followed by 1000 cycles of energy minimization.

Molecular Dynamics Simulations. The SA structures served as starting models for restrained molecular dynamics simulations. To better account for the conformational flexibility, time-averaged restraints were used during the molecular dynamics simulations (Torda et al., 1990; Pearlman & Kollman, 1991; Pearlman, 1994). The characteristic time for exponential decay was 20 ps, and a power of 6 was used for averaging (r^{-6} averaging). The forces were calculated using the "pseudoforce" formulation (Pearlman, 1994). Standard instantaneous restraints were still used, however, during the initial simulated annealing refinement. Indeed, it has been suggested that time-averaged refinement might be less efficient when converging near the true average conformation from initial distance geometry structures (Pearlman, 1994). Each SA structure was submitted to 1.5 ns of *in vacuo* molecular dynamics at 300 K. The SA structure with the lowest molecular mechanics energy was also submitted to a 200-ps molecular dynamics simulation

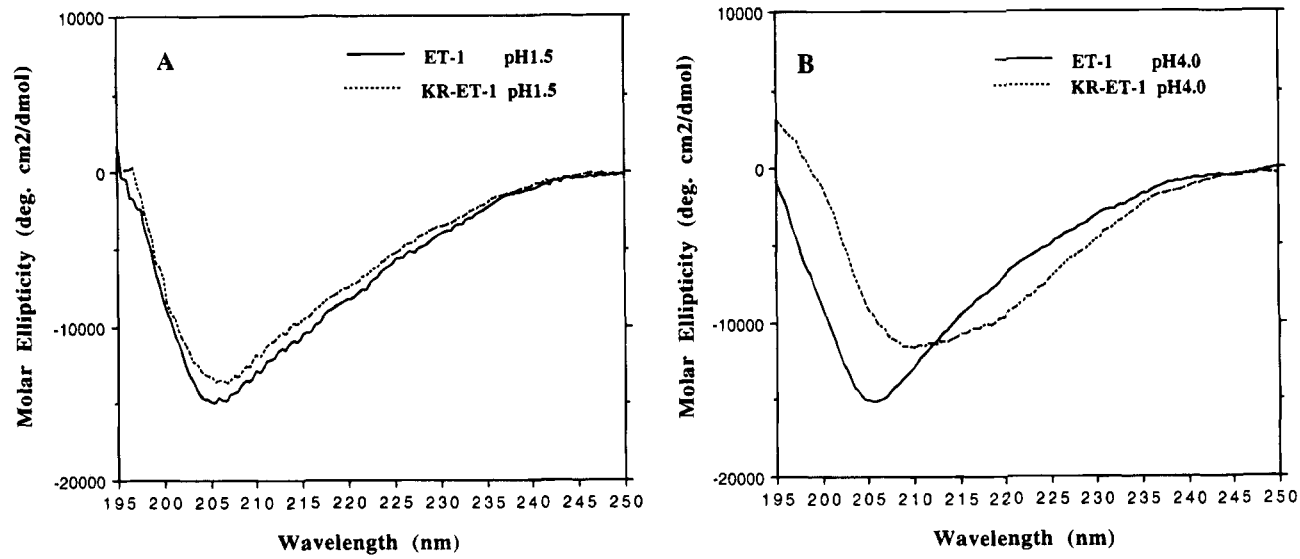

FIGURE 2: CD spectra of ET-1 and KR-ET-1 peptides (A) at pH 1.5 (carboxylic acid state) and (B) at pH 4.0 (carboxylate state). Spectra were recorded in water at 25 °C and at a concentration of 0.02 mM. Each spectrum is the result of the accumulation of 32 scans.

in a 48.5 × 38.5 × 35.6 Å^3 box of water (2089 water molecules) with periodic boundary conditions and a constant pressure (1 atm). The following strategy was used to prepare the system for the MD simulation. The water molecules were first minimized and subjected to 10 ps of MD in the presence of the rigid protein. Then the protein water system was energy minimized in several steps, gradually reducing the positional constraints on the protein backbone from 100 to 0 kcal·mol^{-1}·Å^{-2}. The MD simulation was then started, and the temperature was gradually increased from 10 to 300 K in 15 ps. The system was maintained at this temperature for 185 ps. To avoid local heating effects, separate velocity scaling factors were used for the solute and the solvent. Monitoring the change in the total potential energy (including the pseudoenergy term for NMR constraints) as a function of time indicated that initial equilibration was achieved within 50 ps. Then the potential energy remained essentially constant until the end of the simulation. Hence the MD analysis was performed over the 50−200-ps trajectory. The conformations were saved every 5 ps. The trajectories were visualized with the Insight II program and analyzed with CARNAL (Ross, 1994).

RESULTS

(A) Circular Dichroism. CD spectra of ET-1 and KR-ET-1 recorded in water at pH 1.5 and 4.0 are displayed in Figure 2. At pH 1.5, the two spectra were very similar with a negative band at 206 ± 1 nm. At pH 4.0, the KR-ET-1 spectrum clearly showed a shift of the negative band to 209 ± 1 nm and a distinct shoulder around 221 ± 1 nm while the ET-1 spectrum remained unchanged. This modification in the CD spectrum suggested an increase in the helical contribution. It should be pointed out that ET-1 and KR-ET-1 spectra recorded at pH 7.0 and 9.5 are similar to their pH 4.0 spectra (data not shown).

(B) Nuclear Magnetic Resonance. In contrast to the severe aggregation of ET-1 in water, the KR-ET-1 solution gave lines sharp enough to allow the NMR study to be carried out in water, without apparent aggregation, either in the carboxylate (pH 4.1) or in the carboxylic acid (pH 1.5) state. Nevertheless, signals were very slightly sharper at pH 4.0 and 1.3 when the concentration was reduced 10-fold (0.32 mM).

Taking into account the large changes in the NMR spectrum directly related to the carboxyl group ionization state, a structural study was carried out on the peptide in the carboxylic acid state at pH 1.5 and another one in the carboxylate state at pH 4.1.

(1) Carboxylate State (pH 4.1). (a) Assignments. Several 1D spectra were recorded at different temperatures, ranging from 280 to 310 K. Considering amide signal overlaps, the temperature of 305 K was chosen to record a first set of experimental data (DQF-COSY, TOCSY, and NOESY); then a second set of data was collected at 280 K.

In the 1D spectrum recorded at 305 K and pH 4.1, signals in the low-field area were widely spread. Some amide signals were not well resolved. His16 aromatic signals were easily identified at 8.33 and 7.26 ppm as sharp signals because they are practically temperature insensitive in this pH range. Signals corresponding to Trp21, Phe14, and Tyr13 aromatic protons were present, but their assignment necessitated the aid of DQF-COSY. It is interesting to note that one Cα proton resonance was particularly downfield shifted (5.22 ppm), whereas one methyl signal was more shielded than the others and shifted upfield to 0.45 ppm. The Met7 Cε methyl protons were observed as a sharp resonance at 2.07 ppm. The DQF-COSY map (H_2O, 305 K, pH 4.1) fingerprint region with cross-peak assignments is displayed in Figure 3.

Figure 3 clearly shows 21 NH−CαH cross-peaks for this 23-residue peptide (the Cys3 NH−CαH cross-peak is very weak due to the rapid exchange of its amide proton with the presaturated water signal). Cross-peaks are widely spread from 9.13 (Cys15) to 6.97 ppm (Asp8) for amide protons and from 5.22 (Cys1) to 3.44 ppm (Val12) for Cα proton signals. Asp8 (6.97 ppm) and Leu17 (7.13 ppm) amide signals as well as Val12 (3.44 ppm) and Phe14 (3.73 ppm) Cα proton signals were particularly upfield shifted. From the Cα proton chemical shifts, the corresponding Cβ protons were identified in the CαH−CβH(H′) cross-peak region.

In the TOCSY experiment, 20 spin systems were observed from the amide protons. Among these spin systems, Val12, Glu10, and Met7 were unambiguously identified from their characteristic patterns. The full assignment was done with the standard procedure (Wüthrich, 1986) by combining data from DQF-COSY, TOCSY, and NOESY experiments. Arg-

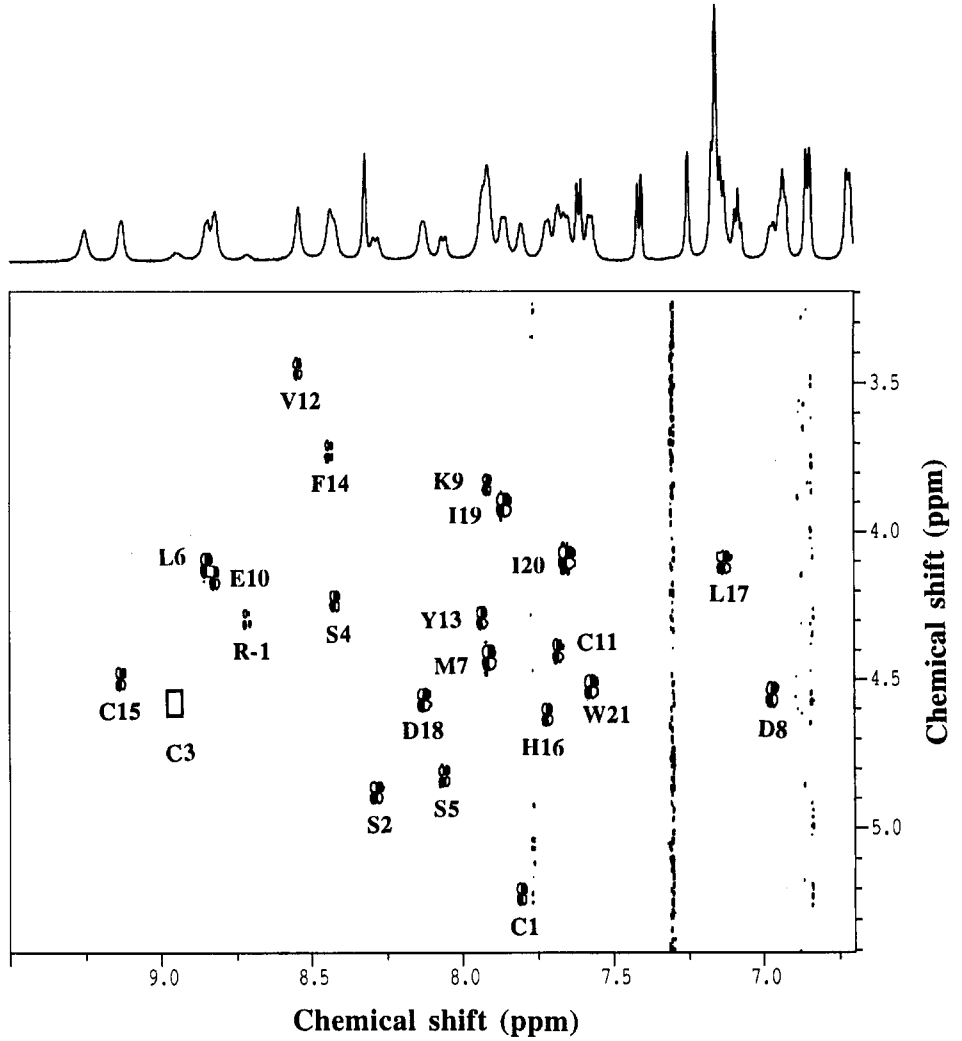

FIGURE 3: Fingerprint region of the 600-MHz DQF-COSY spectrum of KR-ET-1 recorded in water at pH 4.1 and 305 K. The sample concentration was 4.0 mg/0.45 mL. Assignments of the NH−CαH cross-peaks have been indicated. The Cys3 cross-peak position is shown with an open rectangle.

(−1) NεH (9.26 ppm) and CδH_2 (2.56−2.25 ppm) resonances showed highly unexpected chemical shifts (standard chemical shifts are around 7.2 and 3.3−3.2 ppm, respectively). The 6.0 ppm broad signal was assigned to Cη protons of the Arg(−1) guanido group. This signal exhibited low sensitivity to changes in temperature. Chemical shifts and $^3J_{NH-C\alpha H}$ coupling constants measured from DQF-COSY cross-peaks are reported in the supplementary material section.

(b) Amide Proton Exchange and NOEs. The amide proton exchange was followed by recording 1D spectra at increasing times at 290 K and pH 4.8 in deuterated water. After 8−10 h, only five amide protons were still observable. In a NOESY experiment, they were identified as being the Cys11, Val12, Tyr13, Phe14, and Cys15 amide protons and considered as slowly exchanging (Figures 4 and 5).

The main NOE connectivities observed for KR-ET-1 at 280 and 305 K in the carboxylate state, with a mixing time of 180 ms, are displayed in Figure 4 with their relative intensities. The 9−16 helical conformation readily appeared from (i) strong successive d_{NN} NOEs from Leu6 to Leu17, (ii) $d_{\alpha\beta}(i, i+3)$ NOEs in the 9−17 part, (iii) some small $^3J_{NH-C\alpha H}$ coupling constants, and (iv) consecutive slow hydrogen−deuterium amide proton exchanges (from Cys11 to Cys15) (Figure 4). According to β-strand, helix, and coil statistical CαH chemical shifts (Wishart et al., 1991; Lee et al., 1992), the experimental chemical shift versus sequence graph clearly confirmed the helical conformation for the Lys9−Phe14 segment, while the CαH chemical shifts of Cys1 and Ser2 residues were consistent with a β-strand conformation (data not shown).

The Arg(−1) side chain appeared well-defined with several NOEs with Cys11, Phe14, Cys15, and Ile19. Moreover, the three Arg(−1)-Ile19 long-range NOEs, although weak, suggest C-terminal−N-terminal proximity.

(2) pH Titration. Spectra at pHs ranging from 4.8 to 1.3 were recorded at 290 K. Five of these titration spectra with pHs ranging from 2.9 to 1.3 are presented in Figure 5. Clear modifications of the aromatic and methyl regions were induced by protonation of the carboxylate groups of the peptide.

The His16 CεH signal is sharp at pH 2.9, split at pH 1.8, and sharp again at pH 1.3 with a downfield shift of +0.12 ppm. Tyr13 and Phe14 aromatic proton chemical shift changes were analyzed by comparing the pH 2.9 and 1.3 spectra. To highlight these modifications, the characteristic parts of the DQF-COSY are presented in Figure 6. At pH 2.9 the 2,6-H, 3,5-H, and 4-H Phe14 protons are strongly nonequivalent (6.72, 6.92, and 6.52 ppm, respectively) and easily identified by their multiplicity, intensity, and cross-peak pattern in the DQF-COSY map. At pH 1.3 they are strongly downfield shifted by about +0.4 to +0.8 ppm and

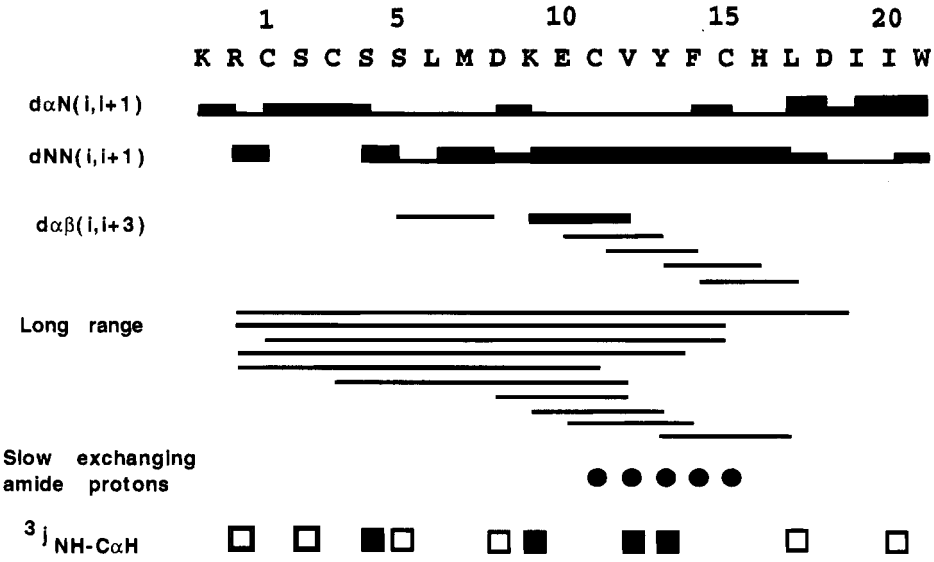

FIGURE 4: Overview of NOE connectivities, $^3J_{NH-C\alpha H}$ coupling constants, and slowly exchanging amide protons of the KR-ET-1 peptide measured in water in the carboxylate state (pH 4.1). The NOE intensities are represented by different bar widths and are classified as strong, medium, and weak. Slowly exchanging amide protons are marked by filled circles. The $^3J_{NH-C\alpha H}$ coupling constants are labeled by filled squares for $^3J_{NH-C\alpha H} \leq 6.8$ Hz and open squares for $^3J_{NH-C\alpha H} \geq 9.0$ Hz.

found as two very close signals at 7.30 ppm (4-H, 2,6-H) and 7.37 ppm (3,5-H).

At pH 2.9, the Tyr13 2,6-H and 3,5-H signals are located at 7.18 and 6.87 ppm while at pH 1.3 they are shifted to 6.85 and 6.73 ppm, respectively (upfield shift of −0.33 and −0.14 ppm). Protonation of carboxylic acid groups can also be followed by the intensity decrease of the Cys1 CαH signal located at 5.22 ppm. This signal is shifted −0.32 ppm upfield in the carboxylic acid state (data not shown). Trp21 aromatic proton chemical shifts were not affected by the C-terminal protonation.

Modifications in the methyl region, concerning mainly Ile19, Leu17, and Val12 residues, are shown in Figure 5. At pH 4.8, a major (≈95%) and a minor (≈5%) Ile19 γMe signal is located at 0.34 and 0.50 ppm, respectively (also seen on the pH 2.9 spectrum of Figure 5). At pH 1.3 the main Ile19 γMe signal is now found at 0.51 ppm while the other one is small and broadened. Intermediate situations appeared in the pH 2.1 and 1.8 spectra. During the pH decrease, we also observed strong signal modifications of Leu17 δMe. The two δMe signals observed at 0.67 and 0.62 ppm at pH 2.9 are downfield shifted to 0.80 ppm at pH 1.3 while the Val12 γMe located at 1.09 ppm at pH 2.9 is upfield shifted to 1.00 ppm at pH 1.3. In addition, in an experiment carried out in H_2O, Arg(−1) Nε and Cδ proton resonances recovered their usual chemical shift values (≈7.2 and 3.3−3.2 ppm, respectively) when the carboxyl group protonation was completed. The Nε proton signal is upfield shifted by about −2.1 ppm while the two Cδ protons are downfield shifted by about +0.6 and +1.0 ppm, respectively. At the end of the titration experiments, a back pH titration confirmed that all these chemical shifts and line-shape changes are reversible, ruling out a disulfide bridge cleavage. Taken together, the intensity and chemical shift changes observed throughout the pH titration allowed us to identify the characteristic spectra of the carboxylic acid and the carboxylate forms and to determine the chemical shifts for the two ionization states. A slow interconversion between these two conformations is clearly required to explain the observation of signals for both species in equilibrium since the reversible protonation of a carboxylate cannot be slow on the ^{1}H-NMR time scale.

This titration experiment showed the influence of the ionization state of the carboxyl groups on the KR-ET-1 NMR spectrum. Arg(−1), Tyr13, Phe14, Leu17, and Ile19 large chemical shift changes strongly suggest different KR-ET-1 conformations for the carboxylic acid and carboxylate states.

(3) Carboxylic Acid State (pH 1.5). To identify the conformational changes induced by carboxyl group protonation, another NMR data set (DQF-COSY, TOCSY, and NOESY) was acquired with KR-ET-1 in the carboxylic acid state in water (pH 1.5, 300 K). The strategy described above enabled full chemical shift assignments.

(4) Acetic Acid/Water Mixture. NMR spectra were also recorded in the 90/10 acetic acid-d_4/water (v/v) mixture to compare KR-ET-1 and ET-1 solution structures (Tamaoki et al., 1991) under the same conditions. The pH of such a KR-ET-1 solution is 2.5. In contrast to the ET-1 results, the 1D spectrum recorded at 290 K, with regard to the Ile19 γMe signal chemical shifts, displayed both the typical carboxylic acid spectrum (≈20%) and the carboxylate spectrum (≈80%) (Figure 7). Spectra recorded at different temperatures ranging from 315 to 280 K showed this percentage to be greatly modified, in a reversible way, suggesting an equilibrium between the two KR-ET-1 conformations. The equilibrium displacement was easily followed by considering chemical shifts and shapes of the Tyr13 and Phe14 aromatic signals and the Ile19 γMe resonances (similar to changes shown in Figure 6). To summarize, the temperature effect on the spectra recorded in the acetic acid-d_4/water mixture was almost equivalent to the pH effect previously observed in water.

The fingerprint region of the DQF-COSY recorded at 290 K confirmed the presence of the two conformations (data not shown). More cross-peaks than expected for a single conformation were observed and divided into a major set (carboxylate form) and a minor set (carboxylic acid form). The NOESY spectrum also supported the presence of an equilibrium since an excessive number of cross-peaks appeared, some of them being located at chemical shifts where only very weak and broad signals were previously present. This cross-peak excess could be due to a slow

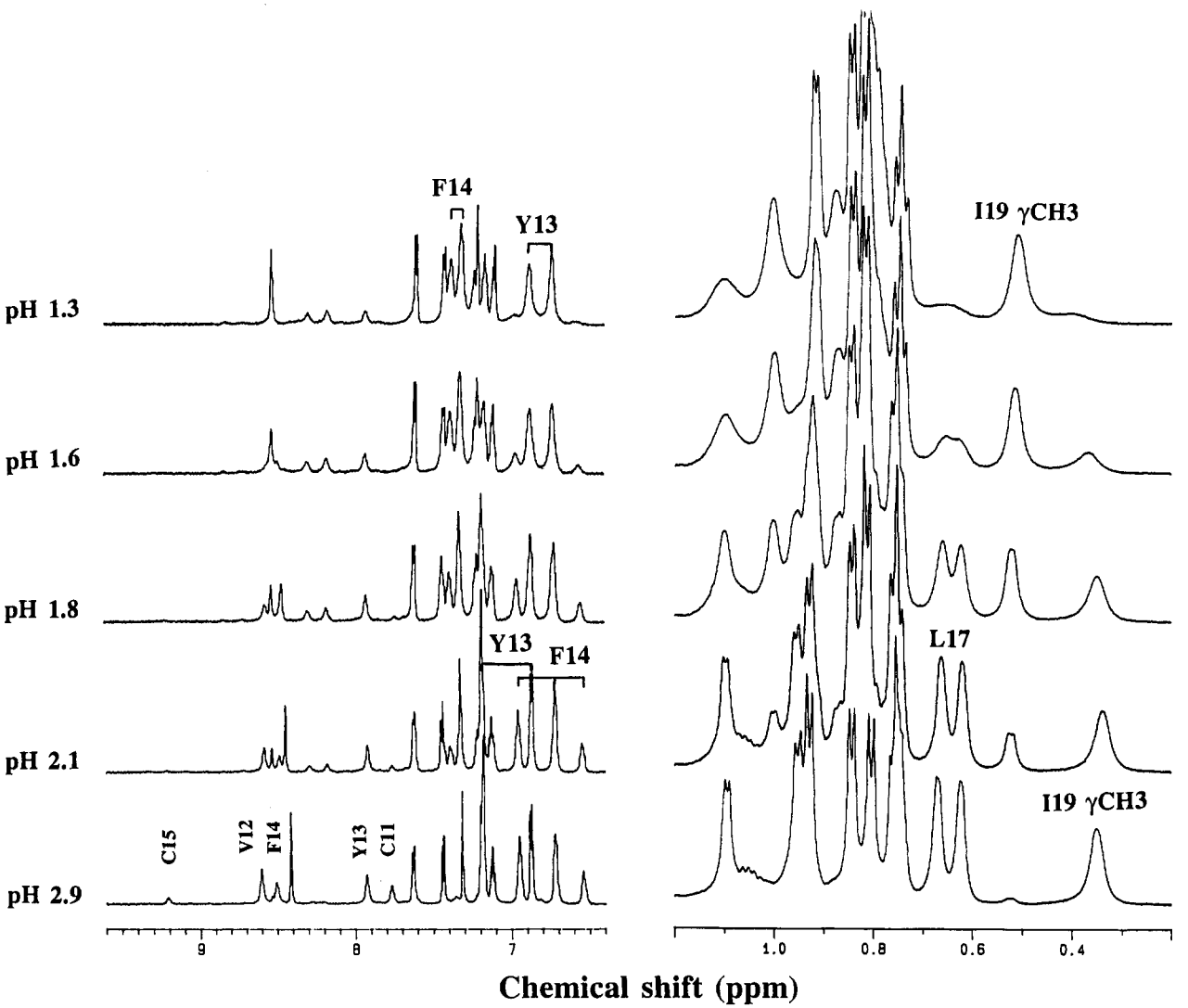

FIGURE 5: Five KR-ET-1 spectra recorded in deuterated water at pHs ranging from 2.9 to 1.3 showing the modifications induced during the protonation of carboxyl groups. Only the low-field and high-field regions in which major changes were observed are displayed. These spectra were recorded after the H−D amide exchange study (290 K and pH = 4.8). Slowly exchanging amide protons are still observed and labeled on the pH 2.9 spectrum. The small signal at 9.20 ppm is the Cys15 amide proton. Three amide protons are still visible at the end of the pH titration experiment (pH 1.3). Tyr13 and Phe14 aromatic protons are labeled in the pH 2.9 and pH 1.3 spectra. In the high-field part, during the protonation of the carboxyl groups, the Ile19 γMe resonance shifts from 0.34 to 0.51 ppm, and Leu17 δMe resonances are shifted from 0.62 and 0.67 to 0.80 ppm. The pH 1.8 spectrum represents an intermediate situation in which His16 C2H and Ile19 γMe resonances roughly show equal carboxylic acid and carboxylate populations.

exchange between the two conformations. To distinguish NOE cross-peaks from cross-peaks due to exchange, a ROESY experiment with a 50-ms mixing time was recorded in which NOE and exchange cross-peaks had opposite signs. Low-field regions of NOESY and ROESY maps are presented in Figure 8, the latter displaying only exchange cross-peaks. It is noteworthy that far fewer cross-peaks due to exchange between minor and major conformations were present in the 280 K NOESY map (data not shown).

In the NOESY map, at 7.30 and 7.37 ppm, both NOE and exchange cross-peaks of the Phe14 aromatic protons are clearly observed. Among these six cross-peaks, only three exchange cross-peaks are observed in the ROESY map. Combining information from the ROESY and the TOCSY and DQF-COSY maps, the chemical shifts of the two conformations could be identified on the same spectrum. These results confirm the KR-ET-1 assignments, both in the carboxylate and in the carboxylic acid states. In addition, the Arg(−1) Nϵ proton chemical shift is so different (9.38 and 7.18 ppm in the carboxylate and carboxylic acid forms, respectively) that it could be indicative of a strong modification in its vicinity. Overall, the large chemical shift differences observed in the acetic acid/water mixture strongly corroborate the results in water which show two different KR-ET-1 conformations in the carboxylic acid and carboxylate states.

It is to be noted that HCl addition to the acetic acid-d_4/water mixture gave a spectrum characteristic of the carboxylic acid form (data not shown).

(C) KR-ET-1 Three-Dimensional Structures. (1) Distance Geometry. The 10 best carboxylic acid and carboxylate KR-ET-1 DIANA structures, in agreement with NMR constraints obtained in water, are displayed in Figure 9.

In the carboxylic state, the helical part spanning residues 9 through 16 is well conserved, while the C-terminal part appears unconstrained (Figure 9A), as reported in most studies on ET-1 and ET family peptides cited above (Coles et al., 1994, and references therein). A mean backbone RMSD value of 1.50 Å was measured from the 1−3 and 9−16 superimposition.

In contrast, distance geometry structures obtained for KR-ET-1 in the carboxylate form show a C-terminal section

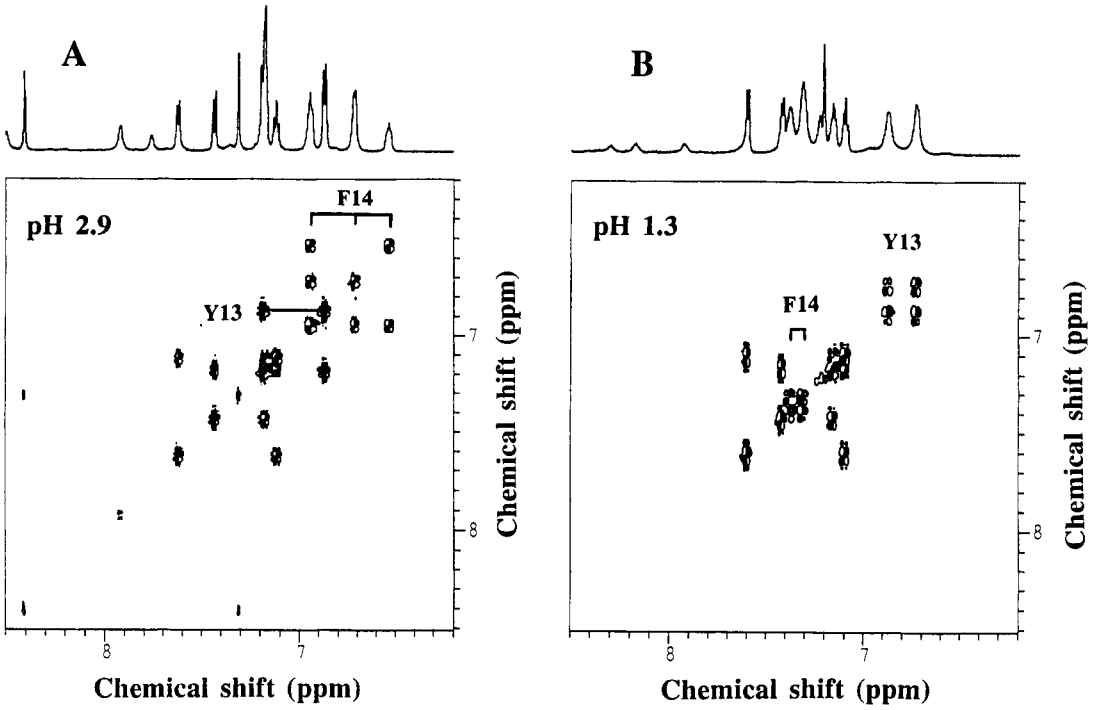

FIGURE 6: pH effect on KR-ET-1 Tyr13 and Phe14 aromatic protons. Throughout the KR-ET-1 pH titration experiment, two DQF-COSY spectra were recorded at pH 2.9 (panel A) and pH 1.3 (panel B). At pH 2.9, Tyr13 aromatic protons are downfield shifted, while Phe14 2,6-H, 3,5-H, and 4-H aromatic protons are upfield shifted and well separated.

folding toward the N-terminus. The mean backbone RMSD value is now 0.89 Å for the 1−3 and 9−16 superimposition. The 3−8 segment is rather well-defined with two successive, slightly twisted, β-turns comprising residues 3−6 and 5−8, the latter segment being stabilized by a hydrogen bond between Asp8 NH and Ser5 carbonyl, although the Asp8 amide proton was not found to slowly exchange. Slowly exchanging Tyr13, Phe14, and Cys15 amide protons were clearly found to hydrogen bond, thus stabilizing the helical part. In addition, an NH(Leu17)−O(Phe14) hydrogen bond was observed in most structures, indicating a helix extension toward the C-terminus. Due to several long-range NOEs [Arg(−1) Hβ,β'−Cys15 Hα, Arg(−1) Hγ,γ'−Cys15 Hα, Arg(−1) Hδ,δ'−Cys15 Hα, Arg(−1) NϵH-Cys11 Hβ,β', Arg(−1) NϵH−Cys11 HN, Arg(−1) NϵH−Phe14 Hϵ, Arg(−1) NϵH−Ile19 δMe, and Arg(−1) NϵH−Trp21 Hζ2], the Arg(−1) side-chain orientation appeared well-defined, its guanido group being located between Glu10/Asp8 and the C-terminus.

To compare the carboxylic acid and carboxylate KR-ET-1 structures, segments 1−3 and 9−16 were superimposed. The mean RMSD per residue of the 10 best structures was then computed and plotted versus sequence numbers (Figure 10A).

(2) Molecular Mechanics and Molecular Dynamics. Molecular dynamics simulated annealing refinement improved both the fit to the NMR data and the molecular mechanics energy. All SA structures had negative molecular mechanics energies and satisfied the NMR data reasonably well with deviations from the imposed restraints smaller than 0.4 Å. The refinement also took into account the electrostatic interactions that cannot be used in distance geometry calculations. In all SA structures, Arg(−1) was salt bridged with Glu10 whereas Lys(−2) interacted with the C-terminus and the side chain of Asp18. The ⟨SA⟩ mean structure displayed in Figure 11 is representative of the salt-bridging arrangements found in the SA structures. RMSDs of the SA structures from their averaged ⟨SA⟩ model are plotted in Figure 10B along with the same values for the molecular dynamics simulations. The observation that the RMSD values are higher for the molecular dynamics runs shows that these simulations allowed better conformational sampling. Figure 12 shows the superimposition of conformations calculated along the molecular dynamics simulation performed on one SA structure, highlighting the mobility of the Arg(−1), Asp8, and Glu10 side chains. Figure 12 also shows that, although less frequent than Arg(−1)−Glu10, the Arg(−1)−Asp8 interaction was not impossible. The percentage of occurrence of main salt bridges in the various simulations is summarized in Table 1.

DISCUSSION

A large number of solution structures of ET family peptides have been reported; these include ET-1 (Tamaoki et al., 1991; Aumelas et al., 1991a; Reily & Dunbar, 1991; Andersen et al., 1992), big ET-1 (Inooka et al., 1991; Donlan et al., 1992), ET-2 (Né et al., unpublished results), ET-3 (Bortmann et al., 1991; Mills et al., 1992), STX (Aumelas et al., 1991b; Mills et al., 1991), and VIC (Aumelas et al., 1992). Most studies clearly showed that the 1−16 part is well organized in a rather rigid core, including a 1−4 extended part and a 9−16 helical part linked together by the 1−15 and 3−11 disulfide bonds, although large flexibility was proposed for the Ser2−Ser5 segment (Andersen et al., 1992). In contrast, the hydrophobic 17−21 C-terminal part exhibited in most cases considerable conformational flexibility. On this basis, it was supposed that the rigid core should remain mainly unaffected by the N-terminal addition of the Lys(−2)-Arg(−1) dipeptide.

(A) Solution Structure of KR-ET-1 in the Carboxylic Acid and Carboxylate States. Comparison with the ET-1 Conformations. The NMR data recorded in water for the carboxylic state of KR-ET-1 are very similar to previous results obtained in various solvent mixtures either for ET-1 (Tamaoki et al., 1991) or for [Nle7]-ET-1 (Aumelas et al.,

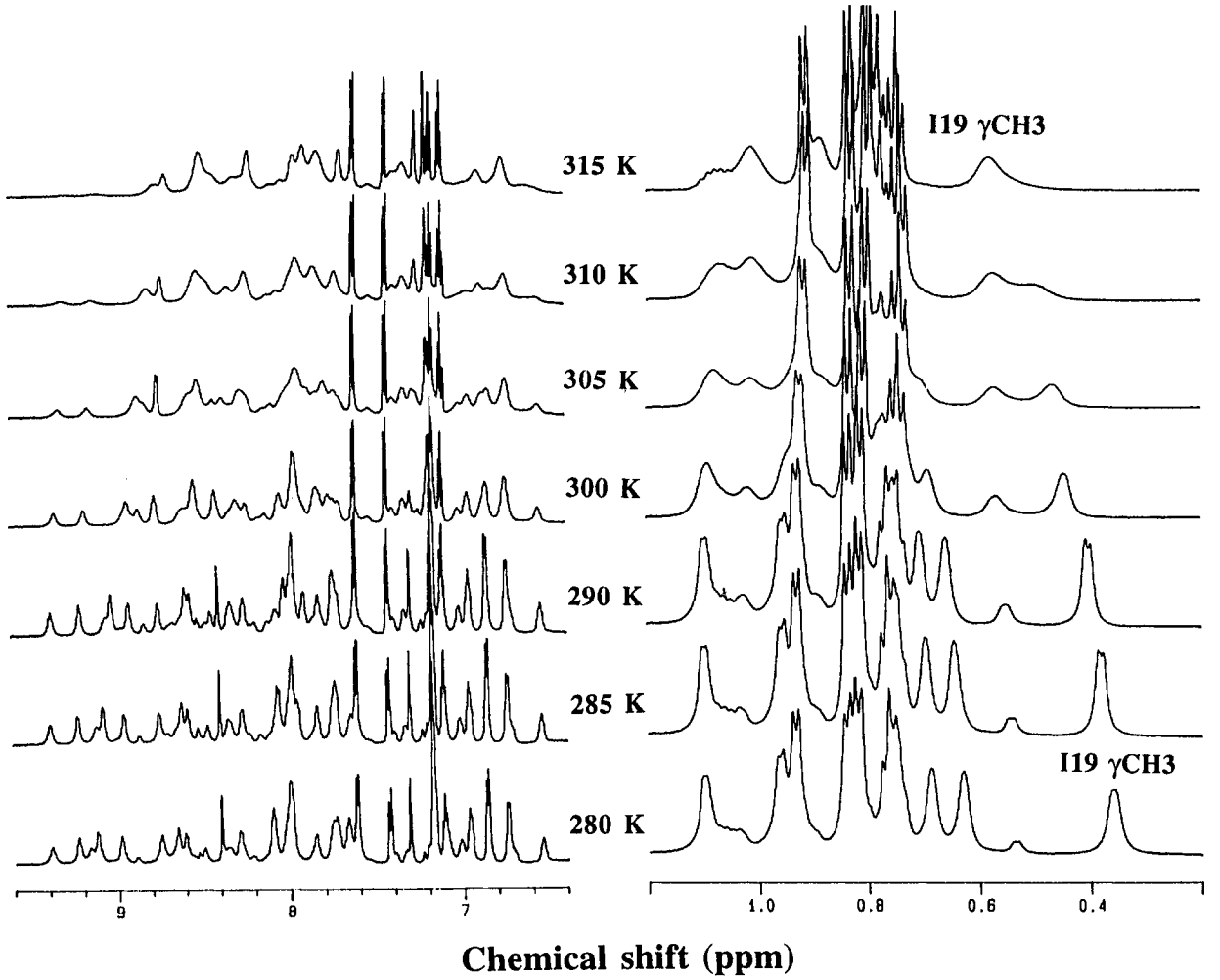

FIGURE 7: Low-field and high-field KR-ET-1 spectra recorded at different temperatures in the 10/90 acetic acid-d_4/H_2O mixture (v/v) at pH 2.5. On the 290 K spectrum, Ile19 γMe (0.41 ppm) and typical nonequivalent Phe14 aromatic resonances allow us to identify the major spectrum (≈80%) as the carboxylate conformation spectrum. The Ile19 γMe (0.55 ppm) is representative of the minor carboxylic acid conformation (≈20%). When the temperature is decreased from 315 to 280 K, amide proton resonances become sharper and more spread out, while the Phe14 and Tyr13 aromatic signal shapes and chemical shifts are strongly modified. In the high-field area, the major Ile19 γMe signal (315 K) shifts progressively from 0.58 to 0.37 ppm due to an equilibrium displacement. At 305 K the two conformations are in equal amounts. The temperature increase in the acetic acid-d_4/water mixture induces spectral changes similar to those observed during protonation of carboxyl groups in the pH titration experiment in water.

1991a). The Cα proton chemical shifts versus sequence plots show a striking similarity (data not shown). KR-ET-1 Phe14 and Tyr13 aromatic proton chemical shifts are sensitive to the ionization state. However, their chemical shifts measured in the carboxylic acid state [Phe14 (3,5-H 7.38 ppm, 2,4,6-H 7.30 ppm) and Tyr13 (2,6-H 6.91 ppm, 3,5-H 6.77 ppm)] are very close to those reported for ET-1 in previous studies [Phe14 (2,4,6-H 7.32 ppm, 3,5-H 7.39 ppm) and Tyr13 (2,6-H 6.89 ppm, 3,5-H 6.73 ppm) (Tamaoki et al., 1991)]. All these facts suggest a conformation very similar to that of ET-1 for KR-ET-1 in the carboxylic acid state. Indeed, the corresponding DIANA structure clearly showed the 9−16 helical part linked by the two disulfide bridges to the 1−3 extended part. As previously reported for ET-1 or [Nle7]-ET-1, the KR-ET-1 C-terminal part was found to be unstructured (Figure 9A).

On the other hand, in the carboxylate state, the larger amide proton chemical shift range is consistent with a modified and more organized three-dimensional structure than in the carboxylic acid structure. Amide protons of Cys1, Cys3, Asp8, Glu10, Cys15, and Leu17 residues displayed wide chemical shift variations ranging from 0.50 to 0.80 ppm. Similarly, the Cα proton chemical shifts of Cys1, Ser2, Cys3, Ser5, and Phe14 residues displayed significant variations ranging from 0.22 to 0.51 ppm. In addition, the strong nonequivalence of Cβ protons of Cys1 (0.71 ppm), Cys3 (0.74 ppm), and Cys15 (0.64 ppm) and the 0.30 ppm nonequivalence observed for those of Cys11 (they are equivalent in the carboxylic acid state) are in agreement with a more rigid conformation for the cystine-stabilized motif.

The KR-ET-1 CD spectra also corroborate the conformational changes observed between the two ionization states and indicate a higher helical contribution in the carboxylate state.

The ϕ and ψ mean value angles for KR-ET-1 in the two ionization states are reported in Table 2. These values indicate a better defined helical section in the carboxylate state than in the carboxylic state as clearly displayed in Figure 9. In addition, Figure 9B clearly shows a well-defined and folded C-terminal part roughly pointing toward the N-terminus. This folding, along with the Arg(−1) side-chain location, constitutes the main modifications between the structures in the carboxylate and carboxylic acid states. Moreover, a hydrophobic cluster [Arg(−1), Val12, Tyr13, Phe14, Leu17, Ile19, Ile20, and Trp21 side chains] and two hydrophilic regions, including Asp18, His16, Lys(−2), and

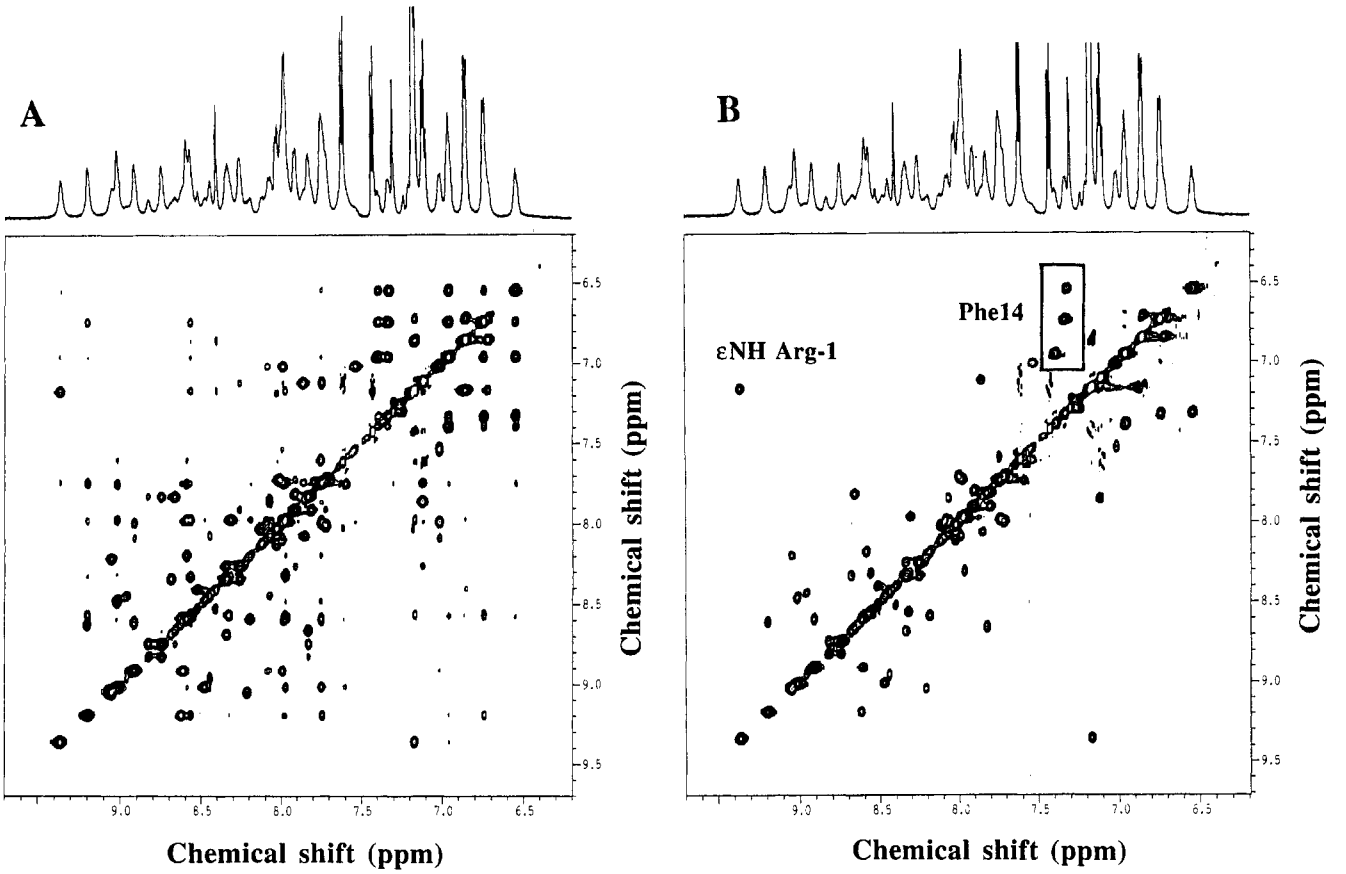

FIGURE 8: KR-ET-1 NOESY (panel A) and ROESY (panel B) low-field areas recorded in the 10/90 acetic acid-d_4/H_2O mixture (v/v) at pH 2.5 and 290 K. The NOESY was recorded with a mixing time of 180 ms and shows both NOEs and exchange cross-peaks. The same area of the ROESY experiment recorded with a mixing time of 50 ms shows only exchange cross-peaks. The 9.38 ppm resonance is assigned to the Arg(−1) Nϵ proton in the carboxylate form. The ROESY exchange cross-peak at 9.38/7.18 ppm reveals the chemical shift of the Nϵ proton in the carboxylic acid form, which is upfield shifted by 2.2 ppm. Phe14 aromatic protons are more spread out in the carboxylate state than in the carboxylic acid state; their exchange cross-peaks are framed in the ROESY map. Other cross-peaks of the ROESY map are mainly due to amide resonance exchanges.

N- and C-termini, on the one hand, and the Arg(−1) δ-guanido group, Asp8, Lys9, and Glu10, on the other hand, can be recognized in the carboxylate KR-ET-1 structures. Compared with ET-1, the strengthening of the two hydrophilic regions by the Lys(−2)-Arg(−1) dipeptide charged groups could be responsible for the decreased aggregation propensity. The Arg(−1) side chain is involved both in the hydrophobic cluster ($C\beta H_2$, $C\gamma H_2$, and $C\delta H_2$) and in the hydrophilic region (δ-guanido group).

Figure 10A clearly shows that, in the carboxylic acid state, the KR-ET-1 C- and N-termini are not well-defined. The mean RMSD value per residue which gradually increases from His16 to Trp21 to reach 11.7 Å indicates the high mobility of the C-terminal part (see also Figure 9A). Similarly, in the N-terminal part, the mean RMSD value increases from Cys1 to Lys(−2) to reach 6.7 Å. In contrast, these two parts appeared more constrained in the carboxylate KR-ET-1 structure with mean RMSD values for Trp21 and Lys(−2) down to 2.9 and 1.5 Å, respectively. In addition, lower RMSD values for KR-ET-1 in the carboxylate state are observed all along the sequence (Figure 10A). Such a pH-dependent C-terminal folding has not been reported as yet for ET-1, although a recent study of ET-1 in water at neutral pH showed a C-terminus folded toward the helical moiety with Ile19 and Trp21 side chains lying close to Tyr13 (Ragg et al., 1994). This folding was ascribed to hydrophobic interactions. These interactions were also supposed to be responsible for the bending of the C-terminus toward the helical part of the ET-3 structure (Mills et al., 1992; Bortmann et al., 1991).

NMR in the 10/90 Acetic Acid/Water Mixture. A KR-ET-1 NMR spectrum was recorded in the acetic acid-d_4/water mixture for comparison with the ET-1 spectrum previously reported in this solvent mixture (Tamaoki et al., 1991). The KR-ET-1 spectrum showed several unexpected modifications, mainly with respect to chemical shifts and line broadening, which would have been difficult to explain had the effect of pH on KR-ET-1 not been studied (see above). First of all, as shown by the presence of two Ile19 γCH_3 signals at 0.42 and 0.55 ppm, the NMR spectrum recorded at 290 K displayed a mixture (≈80/20) of the carboxylate and carboxylic acid forms. Chemical shifts of Tyr13 aromatic protons and Leu17 methyl groups, as well as the nonequivalence of the Phe14 aromatic protons, allowed us to unambiguously determine that the major spectrum corresponded to the carboxylate form.

The observation that the ratio between the two forms varies with temperature in a reversible way clearly suggests that these two forms are in equilibrium. Moreover, the fact that both the carboxylate and the carboxylic acid conformations of KR-ET-1 are observed implies a slow exchange between the two conformations on the ^{1}H-NMR time scale. This conformational exchange has been clearly demonstrated in spectra recorded at several temperatures (Figure 7) and by the ROESY experiment (Figure 8). The displacement of this equilibrium, from the carboxylate to the less structured

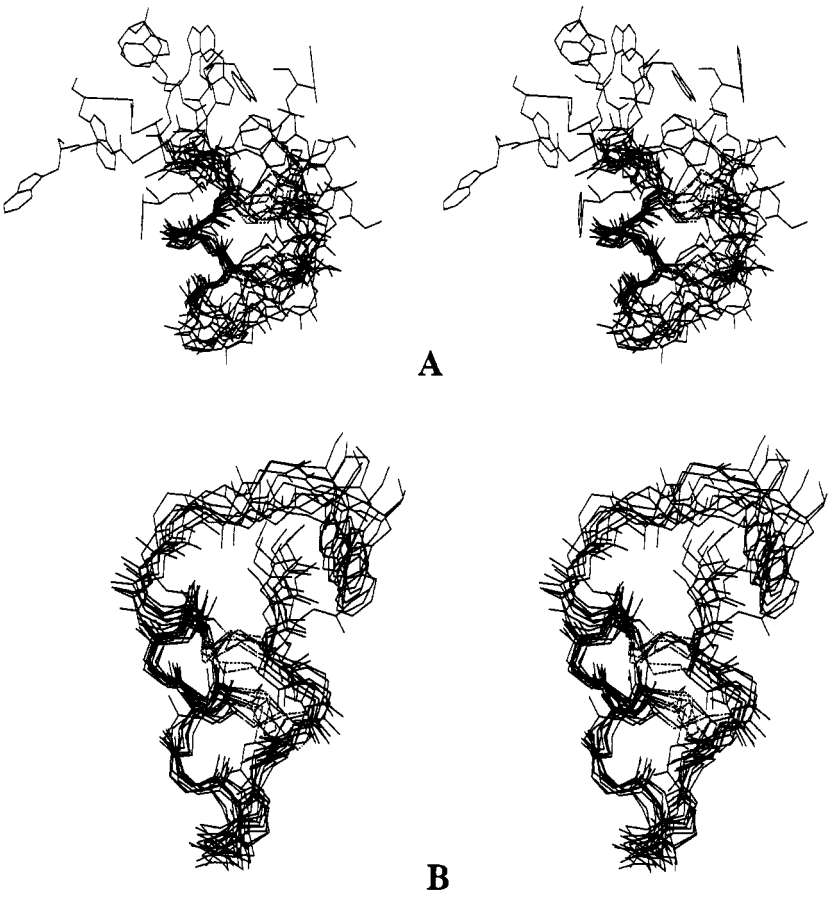

FIGURE 9: Stereoview of the 10 best KR-ET-1 DIANA structures as determined by NMR (A) in the carboxylic acid state (pH 1.5) and (B) in the carboxylate state (pH 4.1). Backbone atoms (N, Cα, C) of residues 1−3 and 9−16 were used to superimpose the structures. For the sake of clarity, only the Trp21 side chain is shown, and disulfide bridges are displayed as dashed lines.

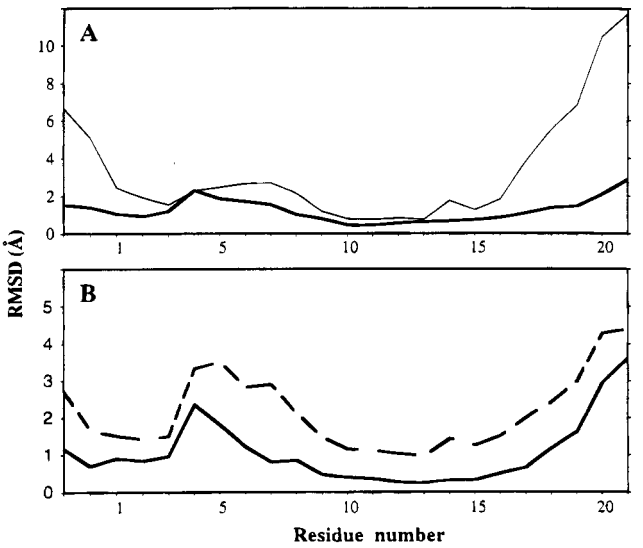

FIGURE 10: Plot of the sequence versus the mean value of RMSDs (N, Cα, C atoms) per residue between individual KR-ET-1 structures and the corresponding average structure. In each set, structures were first translated and rotated to the best superimposition of the backbone atoms (N, Cα, C) of residues 1−3 and 9−16. (A) DIANA structures of the carboxylic acid (thin line) and the carboxylate (thick line) states. (B) Carboxylate state SA structures (thick line) and molecular dynamics trajectories *in vacuo* with time-averaged restraints (thick dotted line).

carboxylic acid conformation with a temperature increase, is probably due mainly to entropic effects. Such an equilibrium might explain the slight line broadening observed rather than aggregation. Indeed, ET-1 was shown to be in the monomeric state in this solvent mixture by ultracentrifugation measurements (Tamaoki et al., 1991). Considering the addition of two hydrophilic residues and the behavior of KR-ET-1 in water, we reasonably believe that there is no aggregation in the acetic acid/water mixture.

Ring Current Effects. With respect to ET-1 (Reily & Dunbar, 1991; Andersen et al., 1992; Tamaoki et al., 1991), ET-2 (Né et al., unpublished results), big ET-1 (Donlan et al., 1992), STX (Aumelas et al., 1991b), and VIC (Aumelas et al., 1992), Phe14 and Tyr13 aromatic protons have typical chemical shifts ranging around 7.2−7.4 ppm for Phe14 and 6.8−6.9 and 6.6−6.7 ppm for Tyr13. In the carboxylic acid state, KR-ET-1 Phe14 and Tyr13 aromatic protons have chemical shifts similar to those of ET-1. In contrast, in the carboxylate state, all Phe14 protons appeared strongly nonequivalent and upfield shifted, while Tyr13 protons resonances were downfield shifted. In addition, Arg(−1) displayed NεH downfield and $C\delta H_2$ upfield shifts when compared to its standard chemical shifts.

On the basis of carboxylate state structures (Figure 11), the Phe14 ring current effect (Perkins 1982) might be responsible for upfield shifts of the Leu17 δCH_3 signals (0.62 and 0.67 ppm at pH 2.9 instead of 0.8 ppm at pH 1.3) due to the helical structure. During carboxylate group protonation, the last helix turn is progressively untightened, and simultaneously the ring current effect is decreased, resulting in a downfield shift of the Leu17 δCH_3 signals.

Similarly, the Arg(−1) side chain appeared rather constrained in the carboxylate state structure and in close proximity to Phe14. The Phe14 ring current effect could therefore explain the atypical Arg(−1) $C\delta H_2$ chemical shifts observed for the carboxylate form.

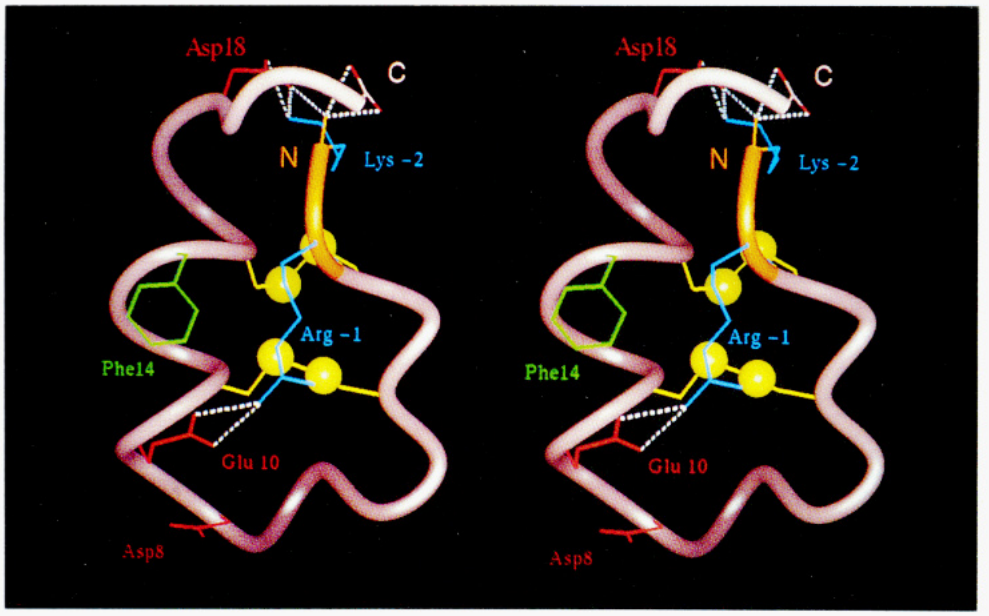

FIGURE 11: Stereoview of the KR-ET-1 average ⟨SA⟩ structure computed *in vacuo*. The Lys(−2)-Arg(−1) dipeptide ribbon is colored in orange. Only selected side chains are displayed. Disulfide bridges are shown in yellow and salt bridges as white dashed lines.

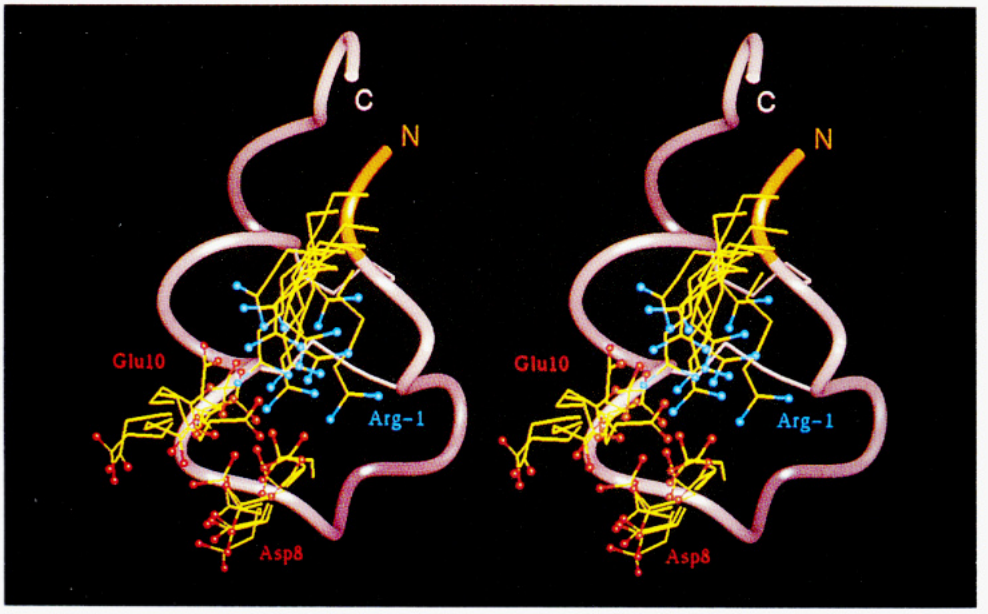

FIGURE 12: Stereoview of 10 conformations of Arg(−1), Asp8, and Glu10 side chains picked along the molecular dynamics simulation (1.5 ns) run on one SA structure *in vacuo* and with time-averaged restraints. The backbone of one of these conformations is displayed as a pink and orange [Lys(−2)-Arg(−1)] curved tube. Oxygen atoms of the Asp8 and Glu10 side chains and guanidine ηN are shown as small spheres. Nϵ of Arg(−1) are colored in yellow as side-chain carbons.

Table 1: Percentage of Salt-Bridge Occurrences in Simulated Annealing KR-ET-1 Structures and in MD Trajectories

conformation set	salt bridge			
	Arg(−1)−Asp8	Arg(−1)−Glu10	Lys(−2)[a]−C-ter	Lys(−2)[a]−Asp18
SA[b]	0	100	80	80
MD *in vacuo*[c]	30	74	96	98
MD in water	0	8.5	0	17

[a] Salt bridges involving either the N-terminus or the Lys(−2) side chain. [b] The 10 SA structures are considered. [c] Trajectories obtained from the 10 SA structures were merged to calculate the percentage of salt-bridge occurrences.

For all ET family peptides, a shielding of the Ile19 γCH$_3$ (between 0.5 and 0.6 ppm) has been observed and has been ascribed to the Trp21 ring current effect. For KR-ET-1 a similar chemical shift was observed in the carboxylic state (0.54 ppm). However, in the KR-ET-1 carboxylate state, the Ile19 γCH$_3$ appeared even more shielded (0.45 ppm), suggesting a stronger Trp21 ring current effect probably due to a more stable C-terminal folded conformation supported by several long-range NOEs between Phe14, Ile19, Trp21, and Arg(−1) residues.

(B) Importance of Electrostatic Interactions in the KR-ET-1 Conformation. (1) NMR and CD pH Titration. The CD and NMR results clearly support participation of the carboxylate groups in KR-ET-1 conformation. In addition, the fact that pH 9.5 and 4.0 CD spectra are the same is indicative of the essential involvement of positive, high pK_a groups such as Lys(−2) (p$K_a \approx 10.4$) or Arg(−1) (p$K_a \approx$ 12) in these electrostatic interactions rather than His16 or the N-terminus whose pK_a's are around 6−7.

Table 2: Angular RMSD Distribution and Standard Deviations of ϕ, ψ Angles for KR-ET-1 Structures in the Carboxylic Acid and Carboxylate States[a]

	carboxylic acid form[b]		carboxylate form[c]	
residue	ϕ (deg)	ψ (deg)	ϕ (deg)	ψ (deg)
Lys(−2)		113.0 ± 37.0		147.6 ± 12.2
Arg(−1)	22.5 ± 77.6	107.0 ± 30.9	−83.1 ± 5.6	−42.8 ± 15.4
Cys1	151.8 ± 71.0	141.3 ± 52.4	−35.3 ± 31.7	57.4 ± 54.4
Ser2	−21.2 ± 76.3	9.4 ± 66.3	−75.4 ± 51.7	37.8 ± 26.4
Cys3	−69.7 ± 70.7	−154.2 ± 70.0	−90.8 ± 35.5	85.0 ± 42.1
Ser4	64.5 ± 57.3	45.5 ± 16.9	−51.6 ± 13.5	−44.8 ± 16.2
Ser5	−68.6 ± 50.3	−81.7 ± 71.0	−85.9 ± 17.1	58.9 ± 27.3
Leu6	118.9 ± 52.9	57.8 ± 20.6	−54.6 ± 34.6	−13.3 ± 22.3
Met7	−166.2 ± 47.4	−52.1 ± 55.0	−58.0 ± 7.9	−39.4 ± 2.8
Asp8	−85.3 ± 49.3	−39.4 ± 38.3	−78.2 ± 4.6	−124.1 ± 20.3
Lys9	93.6 ± 47.4	−12.4 ± 60.5	−62.1 ± 31.2	−28.1 ± 12.0
Glu10	−39.5 ± 58.7	−40.5 ± 10.0	−51.9 ± 8.8	−67.8 ± 4.7
Cys11	−80.4 ± 18.2	−49.8 ± 10.3	−70.6 ± 4.8	−31.6 ± 3.7
Val12	−53.4 ± 3.7	−33.0 ± 9.7	−54.6 ± 3.5	−29.7 ± 2.3
Tyr13	−72.3 ± 13.3	−3.4 ± 15.8	−58.4 ± 2.3	−71.5 ± 3.7
Phe14	−150.7 ± 11.6	53.7 ± 34.7	−64.0 ± 4.9	−30.1 ± 4.5
Cys15	−141.6 ± 39.1	−74.2 ± 10.1	−56.1 ± 6.3	−51.3 ± 3.9
His16	−100.2 ± 29.2	−53.5 ± 23.1	−74.0 ± 6.9	−13.6 ± 20.7
Leu17	54.1 ± 63.0	60.5 ± 28.2	−97.2 ± 18.8	−153.0 ± 31.5
Asp18	121.3 ± 75.0	62.4 ± 14.0	−130.5 ± 46.2	119.6 ± 44.3
Ile19	−60.7 ± 16.6	159.3 ± 7.8	−62.3 ± 32.8	155.0 ± 6.3
Ile20	−109.8 ± 15.9	67.6 ± 11.3	−97.2 ± 15.6	66.3 ± 32.5
Trp21	−124.3 ± 52.5		−138.2 ± 26.2	

[a] These average angle values are obtained from 10 structures. [b] DIANA structures. [c] Simulated annealing structures.

At this stage, it is reasonable to hypothesize that at least one positively charged side chain of the Lys(−2)-Arg(−1) dipeptide and one or several of the four carboxylate groups (Asp8, Glu10, and Asp18 side chains and the carboxyl terminus) could be involved in electrostatic interactions leading to the KR-ET-1 carboxylate conformation. The length and flexibility of Lys(−2) or Arg(−1) side chains appear particularly well-suited for such interactions. Large Arg(−1) NϵH and CδH$_2$ chemical shift changes observed during carboxylate protonation [while Lys(−2) chemical shifts remained almost unchanged] strongly suggest participation of the δ-guanido group in such an electrostatic interaction. In addition, the Arg(−1) NϵH signal undergoes large chemical shift changes from a low field (9.26 ppm) to a more usual chemical shift (7.14 ppm) during protonation of carboxylic groups. This chemical shift change might be due to the ring current effect of the proximal Phe14 already invoked for the Arg(−1) CδH$_2$. Nevertheless, the chemical shift variation of NϵH was stronger and reversed when compared with CδH$_2$. Similar chemical shift variations for Arg(−1) NϵH have been reported in several peptides and were ascribed to hydrogen bonding of the Arg side chain (Tsikaris et al., 1992, 1993, 1994). Therefore, the behavior of Arg(−1) NϵH in KR-ET-1 strongly suggests the involvement of the Arg(−1) guanido group in the electrostatic interactions. DIANA structures showed that salt bridging of Arg(−1) with either Asp8 or Glu10 was likely.

In an attempt to identify which carboxylate group was interacting with the Arg(−1) δ-guanido group, CαH, CβH$_2$, and CγH$_2$ chemical shifts of Asp8, Glu10, Asp18, and Trp21 residues, all bearing carboxylate groups, were examined. When the C-terminal carboxyl group is deprotonated, upfield chemical shifts around −0.2 ppm are usually measured for the CαH. Asp Cβ and Glu Cγ protons are more sensitive to deprotonation, and chemical shift variations of −0.3 ppm are usually expected. The observed Trp21 CαH (−0.18 ppm) and Asp18 CβH$_2$ (−0.32, −0.33 ppm) upfield chemical shift variations are similar to expected values. On the other hand, larger and unexpected variations were observed for Asp8 CβH$_2$. The CβH was downfield shifted by +0.27 ppm while the CβH′ was upfield shifted by −0.56 ppm, leading to a 1.07 ppm nonequivalence of the two Cβ protons in the carboxylate state, instead of 0.24 ppm in the carboxylic acid state. In addition, the amide proton signal was found −1.06 ppm upfield. Such huge chemical shift differences could be indicative of a highly constrained Asp8 side chain. Glu10 proton chemical shift variations were weaker as expected for CγH$_2$ (−0.07 and 0 ppm). Nevertheless, equivalent in the carboxylic acid state, Cβ (2.12 ppm) and Cγ (2.50 ppm) Glu10 protons were found to be slightly nonequivalent (by 0.09 and 0.07 ppm, respectively) in the carboxylate state.

(2) Molecular Mechanics Calculations. To improve the potential energy of the carboxylate DIANA structures, and to take into account electrostatic interactions which appeared determinant in the KR-ET-1 conformation, these structures were submitted to energy refinement and molecular dynamics simulations. The KR-ET-1 SA structures displayed a unique salt-bridge arrangement (Figure 11 and Table 1). Nevertheless, two electrostatic interaction areas can be distinguished; the first involves Asp8, Glu10, and Arg(−1) charged groups and the second Lys(−2), Asp18, and the N- and C-terminal charged groups. In these structures, however, which were energy minimized *in vacuo*, the electrostatic interactions are most likely overestimated, leading to poor representation of the conformational flexibility. Molecular dynamics simulations at 300 K with time-averaged NMR restraints led to a better sampling of the available conformational space as shown by the larger RMSDs in Figure 10. Under these conditions, in the first area, Arg(−1) salt bridging was no longer unique but allowed some interplay between Arg(−1)−Glu10 and Arg(−1)−Asp8 interactions (Figure 10 and Table 1). However, the percentage of occurrence of the former was still larger (74% versus 30%; in some cases Asp8 and Glu10 were involved simultaneously) showing that Glu10 is probably the favorite bridging partner of Arg(−1). This result was further strengthened by a 200-ps simulation with explicit water molecules performed on one SA structure. In this case, the only salt bridge found with a significant frequency was the Arg(−1)−Glu10 interaction (8.5%).

On the other hand, in the second area, the salt-bridge arrangement involving Lys(−2) and Asp18 side chains and N- and C-termini remained essentially unchanged during the molecular dynamics simulations, implying a probable particular stability of the electrostatic network shown in Figure 11. However, most salt bridges in this area were lost in the simulation with water except for the Asp18−Lys(−2) (N-terminus) (17%). It should be kept in mind, nevertheless, that the 200-ps simulation in water run on only one SA structure did not provide large conformational screening as did the simulations run *in vacuo*.

Although Asp8 did not appear strongly involved in salt bridging, its side-chain conformation remained strikingly conserved over simulations with a χ1 angle close to 180°. In this conformation, Asp8 is well oriented to hydrogen bond with amide protons of residues 10, 11, or 12, therefore acting as an N-cap for the 9−16 helix (Huyghues-Despointes et al., 1993; Dasgupta & Bell, 1993; Harper & Rose, 1993). This Asp8 conformation also brings one of the Cβ protons in close proximity to sulfur atoms of Cys3 or Cys11, whereas the other Cβ proton is pointing toward the solvent. Such a different environment is probably responsible for the large

nonequivalence of Asp8 Cβ protons observed in the carboxylate state (see above). KR-ET-1 electrostatic interactions taking place both at the helix N-terminus [helix N-capping by Asp8 and the Arg(−1)−Glu10 interaction] and at the helix C-terminus [the carboxylate groups of Asp18 and the C-terminus interacting with positively charged groups of Lys(−2) and the N-terminus] might all contribute to stabilize the helical segment. This hypothesis is consistent with the increase in helical contribution observed in the CD spectra in the carboxylate state as compared with the carboxylic acid state (Figure 2). Helix stabilization by salt bridges has been clearly described for short *de novo* peptides (Marqusee & Baldwin, 1987, 1989) and for the N-terminal fragment of ribonuclease A obtained by CNBr digestion (Bierzinski, 1988).

By weakening all salt bridges, carboxylate group protonation probably provides more flexibility to the N- and C-terminal parts, while the helix is slightly destabilized. Under these conditions, specific ring current effects of the carboxylate conformation are lost, and Arg(−1) chemical shifts recover their usual values while the other chemical shifts become very similar to those of ET-1, in which a large mobility of the C-terminal part has always been reported.

Several conformation stabilizations involving electrostatic interactions have been reported in solution structure studies (Mayer & Lancelot, 1981; Tsikaris et al., 1992, 1993, 1994; Bobde et al., 1993; Scholtz et al., 1993; Zhang et al., 1994; Marqusee & Baldwin, 1987, 1989; Bierzinski, 1988). More generally, salt bridges are found in many native proteins, implying that they have a stabilizing effect (Cantor & Schimmel, 1980). This is given further support by the observation that thermostable proteins display an even larger number of surface salt bridges (Creighton, 1993a).

(C) Possible Implication of Electrostatic Interactions in Native Disulfide Bridge Formation of KR-ET-1. Taken together, our results underscore the importance of electrostatic interactions in Arg(−1) side-chain location and the conformation of the C-terminal part. We are now investigating the extent to which such specific electrostatic interactions might contribute to *in vitro* KR-ET-1 disulfide bond formation.

Generally, protein folding takes place *in vivo* in the most effective manner to yield a bioactive structure, while the *in vitro* pathway sometimes generates both native and non-native compounds (Gilbert, 1994). This is indeed observed for the ET-1 disulfide bond formation, for which the *in vitro* folding gives an ≈3/1 native/non-native ratio regardless of the folding conditions. The large increase in the amount of the native arrangement (ratio ≥9/1), due to addition of the Lys(−2)-Arg(−1) dipeptide found in the KR-ET-1 proendothelin sequence, could suggest an "*in vivo*-like" process for this compound. Since we have shown that electrostatic interactions play a major role in the KR-ET-1 conformation, it is tempting to speculate that they also participate in folding improvement. This hypothesis is furthermore supported by the fact that guanidine hydrochloride, known to weaken electrostatic interactions, was found to abolish the improved disulfide bridge of KR-ET-1 (Kubo et al., manuscript in preparation) while no change was observed in the disulfide bond formation in truncated apamin and sarafotoxin (Ramalingam & Snyder, 1993).

Considering the KR-ET-1 electrostatic interaction network (Figure 11), a good charge complementarity appears between the N-terminal part [N-terminus and Lys(−2) side chain] and the C-terminal part (C-terminus and Asp18 side chain), while the Arg(−1) side chain is involved in a salt bridge with the Glu10 carboxylate group. Assuming an *in vivo*-like process, those electrostatic interactions involving N- and C-termini, no longer present in the precursor protein, are probably less important than interactions occurring between side chains. Arg(−1)−Glu10 and Lys(−2)−Asp18 salt bridges might therefore be involved in stabilization of the native disulfide bonding both *in vitro* and *in vivo*. Salt bridges involving the N- and C- termini could of course afford additional stabilization in the KR-ET-1 *in vitro* folding. Moreover, all these interactions probably cooperate with each other, therefore providing a still stronger overall stabilization (Creighton, 1993b). In contrast, no such stabilizing interactions can take place in native ET-1, resulting in *in vitro* formation of a significant amount of non-native disulfide bridging.

Many peptide hormones are initially synthesized as preproproteins which are processed by proteolytic cleavage of the signal peptide and of the propeptide. This processing generally begins after folding has been completed, and the propeptide sometimes appears necessary for folding, as is the case of insulin (Creighton, 1993c). On the other hand, disulfide bridges usually do not determine the protein conformation but only stabilize further the folded conformation (Creighton, 1993d; Cantor & Schimmel, 1980). The fact that, *in vitro*, ET-1 folds in a 3/1 mixture of native and non-native disulfide arrangements probably indicates that native ET-1 is only marginally thermodynamically more stable than the non-native compound. The addition of a pair of basic residues [Lys(−2)-Arg(−1)] taken from the KR-ET-1 precursor affords extra thermodynamic stabilization of the native compound, most likely via salt bridges Lys(−2)−Asp18 and Arg(−1)−Glu10, therefore improving the native/non-native ratio. Hence, most of the pro-sequence enhancement of ET-1 folding appears to be contained in the Lys(−2)-Arg(−1) basic dipeptide, although the latter segment has to be cleaved for full expression of biological activity.

Selectivities toward either native or non-native ET-1 disulfide arrangement have recently been reported (Hunt et al., 1993). These selectivities resulted from steric hindrance due to replacement of two cysteines by penicillamines (Pen) which destabilizes Pen-Pen pairing. In contrast, the native-like selectivity in KR-ET-1 disulfide pairing seems to result from stabilization of the native disulfide bridge arrangement through salt-bridge formation. On the other hand, some striking native disulfide arrangement selectivities were observed when Tyr13 was replaced by Ala (≥95%) (De Castiglione et al., 1992) or when D residues were introduced in position 2, 9, or 12 (≥98%) (Galantino et al., 1992).

(D) Can the Biological Activity Decrease Be Related to the Conformation of KR-ET-1? By comparison of the conformation of ET-1 with KR-ET-1, it is tempting to speculate that some structure−activity relationship guidelines might explain the KR-ET-1 biological activity decrease. As described above, the major conformational changes involve four residues: Trp21, Asp8, Glu10, and Phe14.

The key role of the C-terminal Trp21 residue was demonstrated by complete loss of activity following its removal (Nakajima et al., 1989a,b) or its replacement by Ala (Tam et al., 1994). In addition, amidation of the C-terminus caused a dramatic decrease in biological activity probably due to the loss of the C-terminal charge (Nakajima et al.,

1989a,b). Because of electrostatic interactions along with hydrophobic interactions, the KR-ET-1 C-terminal conformation appeared more constrained in the carboxylate form than in the carboxylic form, this latter displaying a great mobility just like ET-1. The fact that the key Trp21 residue was located in this constrained part of the molecule allows us to hypothesize that this reduced mobility could also affect the interaction between KR-ET-1 and the ET-1 receptor.

In ET-1 structure−activity relationship studies, the importance of the Asp8 and Glu10 side-chain charges was also demonstrated by the loss of potency when these two residues were replaced in turn by Asn and Gln residues (Nakajima et al., 1989b). Compared with ET-1, in which the total negative charges of Asp8 and Glu10 are available, in KR-ET-1, these charges are practically neutralized because of their involvement either in salt bridges or in hydrogen bonding with the Arg(−1) guanidinium or in an N-terminal helix capping box (Asp8). Consequently, if these charges were of importance for the binding or the induction of the biological response, their decrease might affect the biological activity.

The replacement of Phe14 by the Ala residue clearly showed that Phe14 plays an important role in ET-1 biological activity (Nakajima et al., 1989b; De Castiglione et al., 1992). In the KR-ET-1 carboxylate conformation, the Phe14 environment was greatly modified. In accordance with the large chemical shift changes, the aromatic ring appears more constrained than in ET-1 and less accessible to interact with the ET-1 receptor.

Consequently, we hypothesize that these three significant conformational changes for KR-ET-1 in the carboxylate state at the critical sites for expression of the biological activity might together be responsible for the marked biological activity decrease. However, at present, it appears difficult to evaluate the relative importance of each of these various effects.

CONCLUSION

We have shown that the conformation of KR-ET-1 in the carboxylic acid state is very close to that of ET-1. In contrast, the carboxylate state conformation is characterized by a more constrained C-terminal part folded toward the N-terminus and by a well-defined Arg(−1) side-chain location. Molecular mechanics and dynamics calculations suggest an electrostatic network involving the Lys(−2)-Arg(−1) dipeptide that could explain the more highly organized structure in the carboxylate state. The salt bridges involving the Lys(−2)-Arg(−1) dipeptide of KR-ET-1 are thought to be responsible for the improved native disulfide pairing selectivity. Since the added dipeptide has been taken from the sequence of the precursor protein, it is likely that the selectivity increase arises through an *in vivo*-like process. Unfortunately, the selectivity improvement observed for KR-ET-1 is concomitant with a decrease in its biological activity. The reasons for this remain unclear, although it has been shown that environment and flexibility of the key residue Trp21 are strongly modified in KR-ET-1 (carboxylate form) compared to ET-1. Without better knowledge at the atomic level of the interaction with its receptor and the mechanism for signal transmission, it is difficult to understand the exact role of the Lys(−2)-Arg(−1) dipeptide in the loss of biological activity. We are nevertheless planning to more carefully evaluate the contribution of KR-ET-1 charged groups by activity measurements, folding studies, and conformational analysis of appropriate KR-ET-1 analogues.

ACKNOWLEDGMENT

A. Aumelas gratefully acknowledges the Institute for Protein Research of Osaka University, and the Peptide Institute, Inc., Protein Research Foundation, Osaka Japan, for facilities provided as a visiting researcher in 1992. The authors are grateful to Drs. Harada and Takamoto of the Hitachi Co. for access to their NMR spectrometer and thank Dr. Braud for help in recording CD spectra as well as Drs. Nishimura, Nemoto, Crégut, and Padilla for useful and friendly discussions. The authors are grateful to Dr. Lynn S. Salhi for the English revision.

SUPPLEMENTARY MATERIAL AVAILABLE

Two tables containing chemical shifts of KR-ET-1 measured in water in the carboxylate and carboxylic acid states (2 pages). Ordering information is given on any current masthead page.

REFERENCES

Andersen, N. H., Chen, C., Marschner, T. M., Krystek, S. R., & Bassolino, D. A. (1992) *Biochemistry 31*, 1280−1295.

Aumelas, A., Chiche, L., Mahé, E., Le-Nguyen, D., Sizun, P., Berthault, P., & Perly, B. (1991a) *Int. J. Pept. Protein Res. 37*, 315−324.

Aumelas, A., Chiche, L., Mahé, E., Le-Nguyen, D., Sizun, P., Berthault, P., & Perly, B. (1991b) *Neurochem. Int. 18*, 471−475.

Aumelas, A., Chiche, L., Brun, E., Mahé, E., Le-Nguyen, D., Sizun, P., Berthault, P., & Perly, B. (1992) *J. Chim. Phys. Phys.-Chim. Biol. 89*, 175−181.

Bax, A., & Davis, D. G. (1985a) *J. Magn. Reson. 65*, 355−350.

Bax, A., & Davis, D. G. (1985b) *J. Magn. Reson. 63*, 207−213.

Bennes, R., Calas, B., Chabrier, P. E., Demaille, J., & Heitz, F. (1990) *FEBS Lett.*, 21−24.

Bierzinski, A. (1988) *Int. J. Pept. Protein Res. 32*, 256−261.

Bobde, V., Beri, S., & Durani, S. (1993) *Tetrahedron 24*, 5397−5406.

Bortmann, P., Hoflack, J., Pelton, J. T., & Saudek, V. (1991) *Neurochem. Int. 18*, 491−496.

Cantor, C. R., & Schimmel, P. R. (1980) in *Biophysical Chemistry, Part I: The Conformation of Biological Macromolecules*, pp 291−293, W. H. Freeman and Co., New York.

Coles, M., Munro, S. L. A., & Craik, D. J. (1994) *J. Med. Chem. 37*, 656−664.

Creighton, T. E. (1993) in *Proteins, Structures and Molecular Properties*, 2nd ed., (a) p 303, (b) pp 165−167, (c) pp 79−81, (d) p 248, W. H. Freeman and Co., New York.

Dasgupta, S., & Bell, J. A. (1993) *Int. J. Pept. Protein Res. 41*, 499−511.

De Castiglione, R., Tam, J. P., Liu, W., Zhang, J. W., Galantino, M., Bertolero, F., & Vaghi, F. (1992) in *Peptides, Chemistry and Biology* (Smith, J. A., & Rivier, J. E., Eds.) pp 402−403, ESCOM, Leiden.

Donlan, M. L., Brown, F. K., & Jeffs, P. E. (1992) *J. Biomol. NMR 2*, 407−420.

Erhardt, P. W. (1992) in *Endothelin* (Rubanyi, G. M., Ed.) pp 41−57, Oxford University Press, New York.

Gaeta, F. C. A., Slater, L. B., Sunday, B. R., Miller, J. R., Ramsaur, C. L., Ghibaudi, L., & Chatterjee, M. (1990) in *Peptides: Chemistry, Structure and Biology* (Rivier, J. E., & Marshall G. R., Eds.) pp 264−266, ESCOM, Leiden.

Galantino, M., De Castiglione, R., Tam, J. P., Liu, W., Zhang, J. W., Cristiani, C., & Vaghi, F. (1992) in *Peptides, Chemistry and Biology* (Smith, J. A., & Rivier, J. E., Eds.) pp 404−405, ESCOM, Leiden.

Gilbert, H. F. (1994) in *Mechanims of Protein Folding* (Pain, R. H., Ed.) pp 104−136, IRL Press, Oxford.

Günther, P., Braun, W., & Wüthrich, K. (1991) *J. Mol. Biol. 217*, 517−530.

Harper, E. T., & Rose, G. D. (1993) *Biochemistry 32*, 7605−7609.
Hunt, J. T., Lee, V. G., Liu, E. C. K., Moreland, S., McMullen, D., Webb, M. L., & Bolgar, M. (1993) *Int. J. Pept. Protein Res. 42*, 249−258.
Hurle, M. R., Eads, C. D., Pearlman, D. A., Seibel, G. L., Thomason, J., Kosen, P. A., Kollman, P. A., Anderson, S., & Kuntz, I. D. (1992) *Protein Sci. 1*, 91−106.
Huyghues-Despointes, B. M. P., Scholtz, J. M., & Baldwin, R. L. (1993) *Protein Sci. 2*, 1604−1611.
Inooka, H., Endo, S., Kikuchi, T., Wakimasu, M., Mizuta, E., & Fujino, M. (1991) *Pept. Chem. 28*, 409−414.
Inoue, A., Yanagisawa, M., Kimura, S., Kasuya, Y., Miyauchi, T., Goto, K., & Masaki, T. (1989) *Proc. Natl. Acad. Sci. U.S.A. 86*, 2863−2867.
Janes, R. W., Peapus, D. H., & Wallace, B. A. (1994) *Nature Struct. Biol. 1*, 311−319.
Kobayashi, Y., Takashima, H., Tamaoki, H., Kyogoku, Y., Nakajima, K., Lambert, P., Kuroda, H., Chino, N., Watanabe, T. X., Kimura, T., Sakakibara, S., & Moroder, L. (1991) *Biopolymers 31*, 1213−1220.
Krystek, S. R., Jr., Bassolino, D. A., Novotny, J., Chen, C., Marschner, T. M., & Andersen, N. H. (1991) *FEBS Lett. 281*, 212−218.
Kumagaye, S., Kuroda, H., Nakajima, K., Watanabe, T., Kimura, T., Masaki, T., & Sakakibara, S. (1988) *Int. J. Pept. Protein Res. 32*, 519−526.
Labhardt, A. M., & Grunauer, W. (1990) in *10th European Experimental NMR Conference, Posters Abstracts*, May 28−June 1, pp 69−70, Veldhoven, The Netherlands.
Lee, M. S., Palmer, A. G., III, & Wright, P. E. (1992) *J. Biomol. NMR 2*, 307−322.
Macura, S., Huang, Y., Sutter, D., & Ernst, R. R. (1981) *J. Magn. Reson. 43*, 259−281.
Marqusee, S., & Baldwin, R. L. (1987) *Proc. Natl. Acad. Sci. U.S.A. 84*, 8898−8902.
Marqusee, S., & Baldwin, R. L. (1989) in *Protein Folding, Deciphering the Second Half of the Genetic Code* (Gierash, L. M., & King, J., Eds.) pp 85−94, American Association for the Advancement of Science, Washington, DC.
Mayer, R., & Lancelot, G. (1981) *J. Am. Chem. Soc. 103*, 4738−4742.
Mihara, H., Tomizaki, K., Nishino, N., Fujimoto, T., Tamaoki, H., & Kobayashi, Y. (1994) *Biopolymers 34*, 963−967.
Mills, R. G., Atkins, A. R., Harvey, T., Junius, F. K., Smith, R., & King, G. F. (1991) *FEBS Lett. 282*, 247−252.
Mills, R. G., O'Donoghue, S. I., Smith, R., & King, G. F. (1992) *Biochemistry 31*, 5640−5645.
Nakajima, K., Kumagaye, S., Nishio, H., Kuroda, H., Watanabe, T. X., Kobayashi, Y., Tamaoki, H., Kimura, T., & Sakakibara, S. (1989a) *J. Cardiovasc. Pharmacol. 13* (Suppl. 5), S8−S12.
Nakajima, K., Kubo, S., Kumagaye, S., Nishio, H., Kuroda, H., Tsunemi, M., Inui, T., Kuroda, H., Chino, N., Watanabe, T. X., Kimura, T., & Sakakibara, S. (1989b) *Biochem. Biophys. Res. Commun. 163*, 424−429.
Peapus, D. H., Janes, R. W., & Wallace, B. A. (1993) *J. Mol. Biol. 234*, 1250−1252.
Pearlman, D. A. (1994) *J. Biomol. NMR 4*, 1−16.
Pearlman, D. A., & Kollman, P. A. (1991) *J. Mol. Biol. 220*, 457.
Pearlman, D. A., Case, D. A., Caldwell, J. C., Seibel, G. L., Chandra Singh, U., Weiner, P., & Kollman, P. A. (1991) *AMBER 4.0*, University of California, San Francisco.
Perkins, S. J. (1982) in *Biological Magnetic Resonance* (Berliner, L. J., & Reuben, J., Eds.) Vol. 4, pp 193−336, Plenum Press, New York and London.
Phillips, P. E., Cade, C., Bothelho, L. H. P., & Rubanyi G. M. (1992) in *Endothelin* (Rubanyi, G. M., Ed.) pp 31−40, Oxford University Press, New York.
Ragg, E., Mondelli, R., Penco, S., Boli, G., Baumer, L., & Guaragna, A. (1994) *J. Chem. Soc., Perkin Trans. 2*, 1317−1326.
Ramalingam, K., & Snyder, G. H. (1993) *Biochemistry 32*, 11155−11161.
Rance, M., Sorensen, O. W., Bodenhausen, G., Wagner, G., Ernst, R. R., & Wüthrich, K. (1983) *Biochem. Biophys. Res. Commun. 117*, 479−485.
Reily, M. D., & Dunbar, J. B., Jr. (1991) *Biochem. Biophys. Res. Commun. 178*, 570−577.
Ross, W. S. (1994) *CARNAL program from AMBER 4.1 beta release*, University of California, San Francisco.
Saida, K., Mitsui, Y., & Ishida, N. (1989) *J. Biol. Chem. 264*, 14613−14616.
Scholtz, J. M., Quian, H., Robbins, V. H., & Baldwin, R. L. (1993) *Biochemistry 32*, 9668−9676.
Tam, J. P., Liu, W., Zhang, J., Galantino, M., Bertolero, F., Cristiani, C., Vaghi, F., & De Castiglione, R. (1994) *Peptides 15*, 703−708.
Tamaoki, H., Kobayashi, Y., Nishimura, S., Ohkubo, T., Kyogoku, Y., Nakajima, K., Kumagaye, S., Kimura, T., & Sakakibara, S. (1991) *Protein Eng. 4*, 509−518.
Tamaoki, H., Kyogoku, Y., Nakajima, K., Sakakibara, S., Hayashi, M., & Kobayashi, Y. (1992) *Biopolymers 32*, 353−357.
Torda, A. E., Scheek, R. M., & van Gunsteren, W. F. (1990) *J. Mol. Biol. 214*, 223−235.
Tsikaris, V., Sakarellos-Daitsiotis, M., Panou-Pomonis, E., Detsikas, E., Sakarellos, C., Cung, M. T., & Marraud, M. (1992) *Pept. Res. 5*, 110−114.
Tsikaris, V., Cung, M. T., Panou-Pomonis, E., Sakarellos, C., & Sakarellos-Daitsiotis, M. (1993) *J. Chem. Soc., Perkin Trans. 2*, 1345−1349.
Tsikaris, V., Cung, M. T., Sakarellos, C., Tzinia, A. K., Soterdalou, K. P., & Sakarellos-Daitsiotis, M. (1994) *J. Chem. Soc., Perkin Trans. 2*, 821−826.
van Gunsteren, W. F., & Berendsen, H. J. C. (1977) *Mol. Phys. 34*, 1311−1327.
Weiner, S. J., Kollman, P. A., Le-Nguyen, D. T., & Case, D. A. (1986) *J. Comput. Chem. 7*, 230−252.
Wishart, D. S., Sykes, B. D., & Richards, F. M. (1991) *J. Mol. Biol. 222*, 311−333.
Wüthrich, K. (1986) in *NMR of Proteins & Nucleic Acids*, John Wiley & Sons, New York.
Wüthrich, K., Billeter, M., & Braun, W. (1983) *J. Mol. Biol. 169*, 949−961.
Yanagisawa, M., Kurihara, H., Kimura, S., Tomobe, Y., Kobayashi, M., Mitsui, Y., Yazaki, Y., Goto, K., & Masaki T. (1988a) *Nature 332*, 411−415.
Yanagisawa, M., Inoue, A., Ishikawa, T., Kosuya, Y., Kimura, S., Kumagaye, S., Nakajima, K., Watanabe, T. X., Sakakibara, S., Goto, K., & Masaki, T. (1988b) *Proc. Natl. Acad. Sci. U.S.A. 85*, 6964−6967.
Zhang, S., Lockshin, C., Cook, R., & Rich, A. (1994) *Biopolymers 34*, 663−672.

BI942585D